DEVELOPMENT OF PLATINUM-FREE CATALYST BASED ON PYROLIZED VINAZENE CARBON COMPOSITES FOR FUEL CELLS AND AIR BATTERIES CATHODES

BY

ADEOLA AKEEM AKINPELU

A Thesis Presented to the

DEANSHIP OF GRADUATE STUDIES

KING FAHD UNIVERSITY OF PETROLEUM & MINERALS

DHAHRAN, SAUDI ARABIA

In Partial Fulfillment of the
Requirements for the Degree of

MASTER OF SCIENCE

In

CHEMISTRY

RAJAB 1435

KING FAHD UNIVERSITY OF PETROLEUM & MINERALS

DHAHRAN- 31261, SAUDI ARABIA

DEANSHIP OF GRADUATE STUDIES

This thesis, written by ADEOLA AKEEM AKINPELU under the direction his thesis advisor and approved by his thesis committee, has been presented and accepted by the Dean of Graduate Studies, in partial fulfillment of the requirements for the degree of **MASTER OF SCIENCE IN CHEMISTRY.**

Dr. Belabbes Merzougui
(Advisor)

Dr. Abdalla Jafar Salman Hamdan
Department Chairman

Dr. Mazen Khaled
(Member)

Dr. Salam A. Zummo
Dean of Graduate Studies

Dr. Abdulrahman Al-Betar
(Member)

3/6/14
Date

عمادة الدراسات العليا
DEANSHIP OF GRADUATE STUDIES

Adeola Akeem Akinpelu

2014

DEDICATION

This work is dedicated to ALLAH Subhanau Wata`alla

ACKNOWLEDGMENTS

All praise and gratitude belong to Almighty Allah (Subhanahu Wa Ta`allah) for giving me fortitude and patience to carry out this work. May the peace and blessing of Allah be upon the last Prophet Muhammad (Peace be upon him).

My deep and sincere appreciation goes to my thesis supervisor Dr Belabbes Merzougui, for all I have learnt from him and for his continuous help and support in all stages of this thesis. I would also like to thank him for being an open person to ideas, and for encouraging and helping me to shape my interest and ideas.

I am as well grateful to other thesis committee members: Dr Mazen Khaled and Dr Abdul-Rahman Al-Betar, for their supports, review of the thesis report, and recommendations.

I would like to express my deep gratitude and respect to Dr Zain Yamani: Director Center for Excellence in Nanotechnology (CENT), whose leadership style inspires me and becomes invaluable to me. In the same vein, I am also thankful to CENT lab team headed by Dr Nasir Zamman for their cooperation and understanding.

I would like to acknowledge the financial, academic and technical support of the King Fahd University of Petroleum and Minerals, particularly in the award of a Research Assistanship/Studentship through CENT and Chemistry department. The library facilities and computer facilities of the University have been indispensable more importantly financial support for this project through NSTIP. I also thank the Department of Chemistry for their support and assistance especially the head of department, Dr. Al-

Hamdan Abdallah Jafar.

I must not forget to acknowledge and appreciate technical support of my course/project mate: Mr Bukola Abidemi Saheed, whose numerous inputs at different stages of this research work have been marvelous.

I would like to thank my family, especially my mother and father for always believing in me, for their continuous love and their supports in my decisions.

Last, but by no means least, I have to thank my wife and my little daughter for their patience and understanding and for boosting my morale during difficult time.

Table of Content

LIST OF TABLES

LIST OF FIGURES

LIST OF ABBREVIATIONS

ORR	Oxygen reduction reaction
Pt	Platinum
RDE	Rotating disk electrode
CA	Chrono Amperommetry
XPS	X-ray photoelectron spectroscopy
XRD	X-ray diffraction spectroscopy
FESEM	Field emission scanning electron Microscope.
EDX	Energy dispersive X-ray spectroscopy
BET	Brunauer–Emmett–Teller
PEMFC	Polymer electrolyte membrane
DMFC	Direct methanol fuel cell

ABSTRACT (English)

Full Name : Adeola Akeem Akinpelu

Thesis Title : Development of A Platinum-free Catalyst Based on Pyrolized Vinazene –Crabon Composites for Fuel Cells and Air Batteries Cathodes

Major Field : Chemistry

Date of Degree : April 2014

Oxygen (O_2) is the most abundant element in the Earth's crust. The oxygen reduction reaction (ORR) is also the most important reaction in life processes such as biological respiration, and in energy converting systems such as fuel cells batteries. Generally, the ORR kinetics, especially in the acidic medium, is very slow. In order to speed up the ORR kinetics to reach a practical usable level in fuel cell applications, a highly active and stable ORR is needed. To date, platinum (Pt)-based materials are the most practical catalysts used in fuel cells. However, Pt durability, scarcity as well its high cost hamper commercial application of fuel cells. Nonetheless, extensive research over the past several decades has focused on developing alternative catalysts, including non-noble metal catalysts. Among them, non-precious metal (NPM) catalysts consisting of transition metals (in particular, Fe and Co)-nitrogen complexes on carbon support prepared by high temperature pyrolysis are the most promising approaches at the present time. Yet, today's Fe–N–C catalysts still suffer from low activity and poor durability, especially for

unpyrolysed Fe–N–C systems. It is against this background that we are using novel vinazene based nitrogen precursor to develop highly active Fe-N-C electrocatalysts for ORR using different carbon support, such as (ketjenblack EC-300 (KB), Vulcan XC-72R (Vulcan)). The synthesized catalysts were characterized using electrochemical techniques (RDE, and stationary voltamperometry), BET and spectroscopic techniques (RAMAN, XRD,SEM-EDS, and XPS). The synthesized catalyst based on KB showed better activity than catalyst based on Vul. It also has good activity compared to Pt-based catalyst. However, both catalysts Fe-N-C/KB and Fe-N-C/Vulcan demonstrated very good stability and excellent methanol tolerance.

ملخص الرسالة

الاسم الكامل: اديولا حكيم أكينبيلو
عنوان الرسالة: تطوير محفزخالي من البلاتينيوم بناء على فينزانيم-الكربون لخلية الوقود و كاثود بطارية الهواء

التخصص: الكيمياء
تاريخ الدرجة العلمية: ابريل 2014

الأكسجين (O_2) هو العنصر الأكثر وفرة في القشرة الأرضية. تفاعل اختزال الأكسجين هو أيضا تفاعل الأكثر أهمية في العمليات الحيوية مثل التنفس البيولوجية وأنظمة تحويل الطاقة مثل بطاريات خلايا الوقود. عموما، حركية تفاعل اختزال الأكسجين وخاصة في المنطقة الكاثودية من خلية الوقود بطيء جدا. من أجل تسريع حركية تفاعل اختزال الأكسجين للوصول إلى مستوى قابلة للاستخدام العملي في تطبيقات خلايا الوقود، هناك حاجة إلى محفز الكاثود. حتى الآن، محفزات البلاتين هي الأكثر عملية. ومع ذلك، فإن مشاكل المتانة، الندرة وكذلك التكلفة العالية تعيق التطبيق التجاري لخلايا الوقود.على الرغم من ذلك، ركزت أبحاث مكثفة على مدى العقود القليلة الماضية على تطوير المحفزات البديلة، بما في ذلك المواد الحفازة معادن غير النبيلة. منها معادن حافزة غير ثمينة التي تتكون من المعادن الانتقالية (ولا سيما الحديد والكوبالت) ومركبات النيتروجين المدعمة على الكربون والتي تم تحضيرها عند درجات انحلال حراري عالي والتي تعتبراهم نهج واعد. ومع ذالك, محفزات اليوم حديد-نتروجين-كربون لا تزال تعاني من انخفاض النشاط وضعف قوة التحمل، وخاصة بالنسبة لمحفزات الحديد-النايتروجين-الكربون غير المنحلة حراريا. وإزاء هذه الخلفية التي نستخدمها رواية فاينازينين المعتمدة على النايتروجين للمرة الأولى لتطوير محفزات الحديد-النتروجين-الكربون النشطة للغاية لتفاعل اختزال الأكسجين باستخدام دعامة الكربون (ketjenblack EC-300 (KB), Vulcan XC-72R (Vulcan)). وتميزت المحفزات المصنعة باستخدام تقنيات الكهروكيميائية (RDE وvoltamperometry، BET) والتقنيات الطيفية (رامان، XRD، SEM-EDS، وXPS).

CHAPTER 1

INTRODUCTION

1.1 General Background of Fuel Cell and Batteries

Fuel cells are electrochemical devices that convert chemical energy of the fuel and oxidant directly into electricity and heat with high efficiency. Electrochemical processes in fuel cells are not governed by Carnot's cycle; therefore, their operation is simple and more efficient compared with internal combustion (IC) engines. High efficiency makes fuel cells an attractive option for a wide range of applications, including transportation, stationary, and portable electronic devices such as, consumer electronics, laptop computers, video cameras, etc.[1]

Fuel cells are considered environment-benign technology providing solutions to a range of environmental challenges, such as harmful levels of local pollutants, in addition to providing economic benefits due to their high efficiency. The main advantages of the fuel cells are their pollution-free operation and high energy density.[2] Due to their potential to reduce the environmental impact and geopolitical consequences of the use of fossil fuels, fuel cells have emerged as potential alternatives to combustion engines. All fuel cells consist of an anode, to which the fuel is supplied, a cathode, to which oxidant (e.g oxygen) is supplied, and an electrolyte, which allows the flow ions between the anode and cathode as shown in figure 1 below. The electrolyte should be highly resistive to the electron current. The net chemical reaction is exactly the same as if the fuel were burnt,

but by spatially separating the reactants, the fuel cell intercepts the stream of electrons that flow spontaneously from the fuel to the oxidant and diverts it for use in an external circuit.

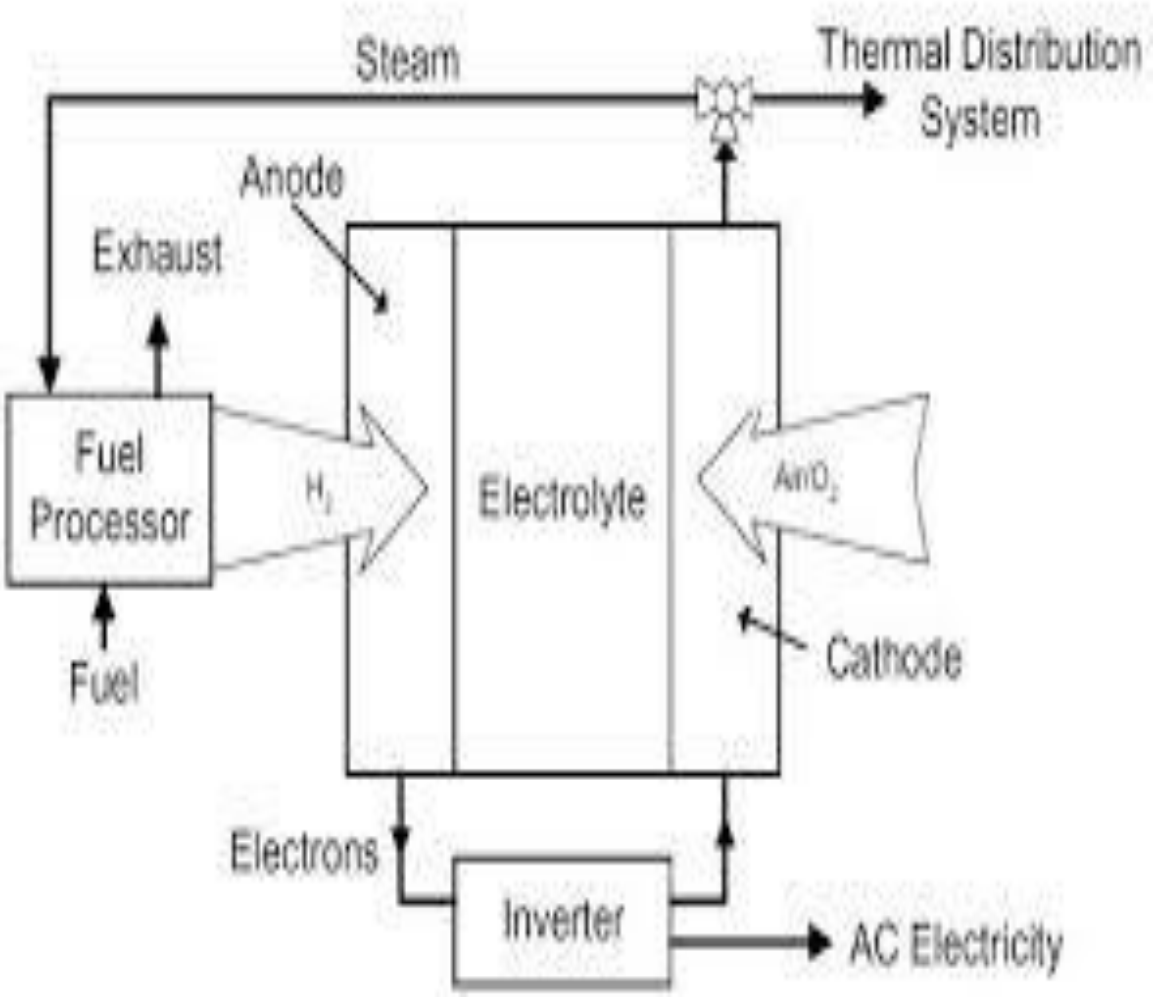

Figure 1: Fuel Cell Schematic Diagram

The fundamental driving force behind this process of ion migration is the concentration gradient between the two interfaces (electrode –electrolyte). The difference between a fuel cell and a conventional battery is that the fuel and oxidant are not integral parts of a fuel cell, but instead are supplied as needed to provide power to the external load. A fuel cell is "charged" as long as there is a supply of fuel to the cell, so self-discharge is absent.

However, these are complicated systems and the voltage output of the typical polymer electrolyte membrane fuel cell (PEMFC) is around 0.7 V only.[3] For many years it was attempted to develop fuel cells as a power source. In the beginning they were developed mainly for space and defense applications. Attempts to develop earth-based systems were made during 1980s and 1990s. Presently fuel cell technology is maturing toward commercialization, but work still needs to be done in many fields. For commercial applications, component materials need to be developed and optimized to improve performance and lower costs.[1] Long-term testing has to be done to obtain information on fuel cell performance.

1.2 Fuel Cell Classification

Fuel cells are classified based on the type of electrolyte they use. The six most common fuel cell types are:

1. Polymer electrolyte membrane fuel cells (PEMFC)
2. Direct methanol fuel cells (DMFC)
3. Alkaline fuel cells (AFC)
4. Phosphoric acid fuel cells (PAFC)
5. Molten carbonate fuel cells (MCFC)
6. Solid oxide fuel cells (SOFC)

1.2.1 Polymer electrolyte membrane fuel cells (PEMFC)

Electrolyte: water-based, acidic polymer membrane

• Also called polymer electrolyte membrane fuel cells

• Use a platinum-based catalyst on both electrodes

• Generally hydrogen fuelled

• Operate at relatively low temperatures (below 100 °C)

• High-temperature variants use a mineral acid-based electrolyte and can operate up to 200 °C.

• Electrical output can be varied, ideal for vehicles

1.2.2 Direct methanol fuel cells (DMFC)

Electrolyte: polymer membrane (like PEMFC)

• Use a platinum–ruthenium catalyst on the anode and a platinum catalyst on the cathode

• This catalyst can draw hydrogen atoms from liquid methanol, which is used as fuel instead of hydrogen, giving the cell its name.

• Operate in the range from 60 °C to 130 °C

• DMFC is convenient for portable power applications with outputs generally less than 250W

1.2.3 Phosphoric acid fuel cells (PAFC)

Electrolyte: liquid phosphoric acid in a bonded silicon carbide matrix

• Use a finely dispersed platinum catalyst on carbon

• Quite resistant to poisoning by carbon monoxide

• Operate at around 180 °C

• Electrical efficiency is relatively low, but overall efficiency can be over 80% if the heat is used

• Used in stationary power generators (100kW to 400 kW)

1.2.4 Alkaline fuel cells (AFC)

Electrolyte: alkaline solution such as potassium hydroxide in water

• Commonly use a nickel catalyst

• Generally fuelled with pure hydrogen and oxygen as they are very sensitive to poisoning

• Typical operating temperatures are around 70 °C

• Can offer high electrical efficiencies

• Tend to have relatively large footprints

• Used on NASA shuttles throughout the space program.

1.2.5 Molten carbonate fuel cells (MCFC)

Electrolyte: a molten carbonate salt suspended in a porous ceramic matrix

• A precious metal catalyst is not necessary

• Can run on hydrocarbon fuels such as methane

• Operate at around 650 °C

• Best run continuously due to the high operating temperature

• Most fuel cell power plants of megawatt capacity use MCFCs, as do large combined heat and power plant

1.2.6 Solid oxide fuel cells (SOFC)

Electrolyte: solid ceramic, such as stabilised zirconium oxide

• A precious metal catalyst is not necessary

• Can run on hydrocarbon fuels such as methane

• Operate at very high temperatures, around 800 °C to 1,000 °C

• Best run continuously due to the high operating temperature

• Popular in stationary power generation [1]

1.3 Oxygen Reduction Reaction

Oxygen (O_2) is the most abundant element in the Earth's crust. The oxygen reduction reaction (ORR) is also the most important reaction in life processes such as biological respiration, and in energy converting systems such as fuel cells. In fuel cell application oxygen is an oxidant that oxides fuel ions, H^+, coming from anode to form in most cases water. ORR in aqueous solutions occurs mainly by two pathways: the direct 4-electron reduction pathway from O_2 to H_2O, and the 2-electron reduction pathway from O_2 to hydrogen peroxide (H_2O_2). In non-aqueous aprotic solvents and/or in alkaline solutions, the 1-electron reduction pathway from O_2 to superoxide (O_2^-) can also occur. In proton exchange membrane (PEM) fuel cells, including direct methanol cells (DMFCs), ORR is the reaction occurring at the cathode. Normally, the ORR kinetics is very slow. In order to speed up the ORR kinetics to reach a practical usable level in a fuel cell, a cathode catalyst is needed. At the current stage technology, platinum (Pt)-based materials are the most practical catalysts. Because these Pt-based catalysts are too expensive for making commercially viable fuel cells, extensive research over the past several decades has focused on developing alternative catalysts, including non-noble metal catalysts. These electrocatalysts include noble metals and alloys, carbon materials, quinone and

derivatives, transition metal macrocyclic compounds, transition metal chalcogenides, transition metal carbides.[4]

Among the non-precious catalysts studied, iron complexed nitrogen on carbon, Fe–N–C, have attracted the most interest owing to their activity, low-cost, and facile preparation methods.[5] However, today's Fe–N–C catalysts still suffer from its low activity and poor durability, especially for unpyrolysed Fe–N–C catalysts. The typical cycle life for unpyrolysed Fe–N–C catalysts is less than 100 cycles in either acidic or basic media.[6] It is a great challenge to replace Pt-based catalysts by inexpensive Fe–N–C catalysts, while maintaining similar performance in practical applications. Metal macrocycles, such as metal (iron or cobalt) porphyrins and phthalocyanines, are the precursors most widely used to prepare the ORR catalysts. To date, however, limited progress has been made in improving their electrocatalytic activity and durability.[7] In particular, macrocycle compounds have been demonstrated for a long time to suffer from severe degradation in fuel cell environments due to demetalation and/or degradation of iron phthalocyanine (FePc) by ORR intermediates.[7]

In any case, the catalytic activity of transition metal macrocyclic compounds towards ORR strongly depends on the individual transition metal center and the macrocyclic ligands, as well as the size of the π electron system. Catalytic compounds studied previously include Fe, Co, Ni, and Cu, and the macrocyclic ligands include chelating atoms N_4, N_2, O_2, N_2 S_2, O_4, and S_4. The conjugate π electron compounds usually include metal phthalocyanine and porphyrin, as well as their derivatives. The activity of these compounds changes with respect to the central metal ions in the following order: Fe>Co>Ni>Cu. For a metal center, the chelating atoms of the macrocyclic ring can also

alter the ORR activity. For example, the active sequence of Fe complexes is as follows: N_4 >N_2O_2 >N_2S_2 >O_4 ≈S_4 (inactive); for Co centers: N_2O_2 > N_4> N_2S_2> O_4≈ S_4; for Cu centers: N_4> O_4 > N_2O_2> N_2S_1> S_4 (inactive); and for Ni centers: O_4 > N_2O_2> N_2S_2> N_4. With respect to these active sequences, recent research has mainly focused on Fe and Co centers, and for macrocyclic rings, on the N_4 system.[4]

It is against this background, the proposed study will focus on developing Fe-N_4/N_x-C catalyst. This will involve impregnation of Nitrogen rich source (Vinazene) on Carbon support (Ketjenblack and Vulcan) followed by complexation of Iron source (Iron(iii)chloride, $FeCl_3$) to produce - under heat treatment in inert atmosphere Fe-N_x-C active sites supported on carbon.

To get insight into understanding the activity behavior of the synthesized catalysts, investigation of their activity, stability, composition, surface area and morphology using electrochemical techniques (RDE, and voltamperometry), BET and spectroscopic techniques (RAMAN, XRD,SEM-EDS, and XPS) was carried out.

CHAPTER 2

LITERATURE REVIEW

2.1 Development of Non-noble Metal Electrocatalyst

Since the first report on non-noble metal catalyst by Jasinski[8] in 1964, development of Pt free catalyst for oxygen reduction reaction has been evolving through different directions. In one embodiment, carbon materials are identified to have some electrocatalytic activity towards ORR.[9] As such, Taylor and Humffray[10] in1975 reported electrocatalytic reduction behavior of ordinary glassy carbon, while related work was also reported by Appel et al[11] in 1978 by using active carbon on glassy electrode. Meanwhile, efforts had been developed to improve the activity of carbon catalyst through pre-treatment. As a result, Marcos and Yeager[12] in 1970 were reported to have studied O_2 reduction on pyrolized graphite while similar study was also done by Paliteiro et al.[13] in 1987.

More recently, Jurmann et al.[14] also reported in 2006 the electroreduction of oxygen on multi-wall carbon nanotubes modified pyrolitic graphite.

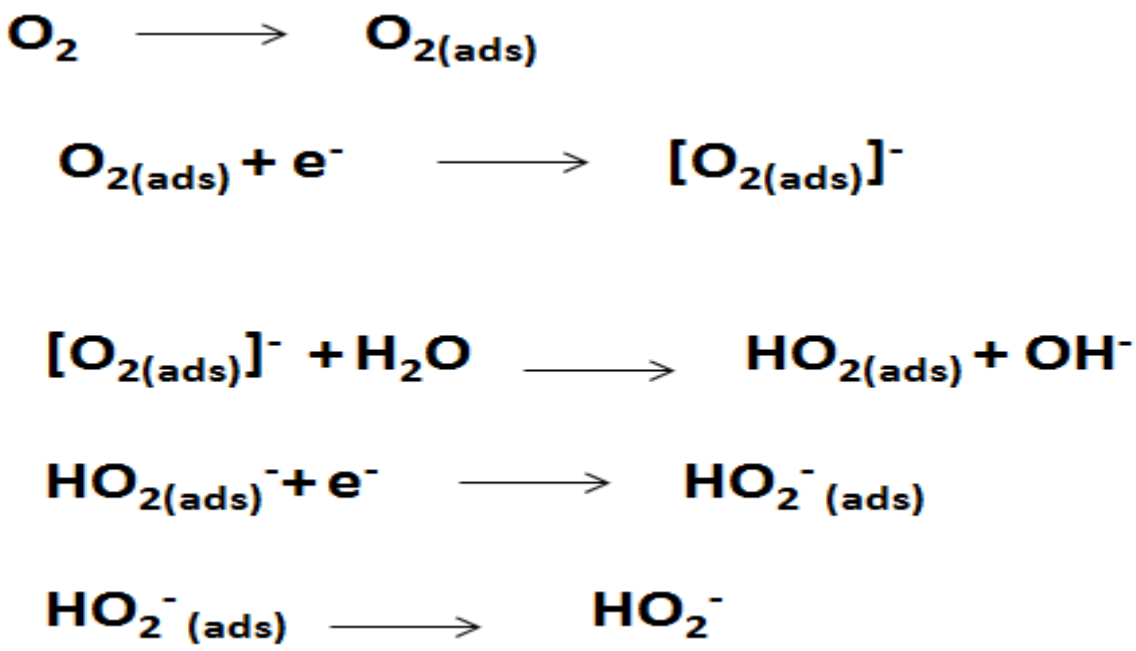

Scheme 1: mechanism proposed by Yeager et al [9] on carbon catalysed oxygen reduction reaction

In another embodiment, doping carbon with heteroatoms such as nitrogen can change or improve electrocatalytic activity of carbon,[4] because nitrogen can withdraw electron from the adjacent carbon which creates net positive charge on the adjacent carbon making it a site for oxygen adsorption and to attract electron from the anode thereby facilitating oxygen reduction reaction. In other word it is termed metal free electrocatalysts.

Jahnke et al.[15] in 1976 reported that N_20_2-, 0_4-, N_2S_2- and S_4-chelates, are able to catalyze the reduction of oxygen, though they are considerably less active than the N_4-compounds. In specific term, Maldonado et al.[16] in 2005 reported the influence of nitrogen doped carbon nanofiber electrode on oxygen reduction, while similar investigation was also reported on nitrogen doped graphite by Sidik et al. [17] in 2006. Recently, metal free electrocatalysts have been deeply investigated. In 2009, Gong et al.[18] reported better electrocatalytic activity of vertically aligned nitrogen containing carbon nanotubes (VA-

CNT) and the said catalyst displayed long term-operation stability and better tolerance to cross over effect than platinum. In similar vein, Qu et al.[19] in 2010 reported good electrocatalytic behavior of nitrogen doped graphene for oxygen reduction reactions. In an amazing development, Yang et al.[20] reported in 2011 sulfur doped graphene as an efficient metal free electrocatalyst for oxygen reduction reaction. Also, relationship between polypyrrole morphology as metal free catalyst and electrochemical activity for oxygen reduction reaction was investigated and reported by Morozan et al. [21] in 2012. Similar investigation was also reported by Unni et al.[22] in 2012. In 2013 efforts were also made to develop efficient metal free catalysts. For example, Shin et al.[23] in 2013 reported electrocatalytic oxygen reduction reaction on electrospun nitrogen-carbon species, while in another development, Jeon et al.[24] in 2013 reported edge-halogenated graphene nanoplatelets as an efficient metal free electrocatalyst for oxygen reduction reaction.

In the third embodiment, although the bid towards platinum free electrocatalysts actually started with metal/nitrogen/carbon composite by Jasinski[8] in 1964, notwithstanding it still appears to be the best among the studied Pt-free catalysts. Transition metal macrocyclic complexes can catalyse O_2 reduction through 2- or 4- electron pathway. In some cases, it can be through both 2- and 4- electron pathways.[4]

In the first instance, Jahnke et al. [15] in 1976 reported that all the experimental results point to the conclusion that, with electrocatalysts, as with natural oxygen carriers, the interaction essential for catalysis takes place between the oxygen and the central metal ion, while also in 1977 Zagal et al.[25] reported oxygen reduction reaction of Co(II) tetrasulfonatephthalocyanine irreversibly adsorbed on a stress annealed pyrolytic graphite electrode surface. In another study by Shigehara and Ason [26] in 1982, the duo reported

the oxygen reduction to form peroxide and further reduction of peroxide to form water at more negative potential by three iron porphyries on graphite electrode while Liu et al [27]in 1983 reported the dependence of oxygen reduction reaction of cofacial cobalt porphyrin on the catalyst structure. It was also reported in 1990 by Shi and Anson [28] the catalytic pathways for the electroreduction of O_2 by iron terakis(4-N-methylpyridyl) porphyrin or iron tetraphenylporphyrin adsorbed on edge plane pyrolytic graphite electrodes. Normally, transition metal macrocyclic complexes do not have long-term stability, especially in concentrated acidic or alkaline solutions. It has been found that thermal treatment of these compounds after they have been adsorbed on high-surface area carbon support particles in the temperature range 450-900 ^{o}C not only increases their stability but also improves their activities.[4] As such, this was supported in the reports of Yeager [9] in 1986 and Zhang et al [29] in 2006.

More recently, Li et al [30] in 2012 reported an excellent oxygen reduction reaction activity of an electrocatalyst base on carbon nano-tube-graphene complexes which contains nitrogen and small amount of iron. Merzougui et al[31] in 2013 also reported an impressive activity and stability of another electrocatalysts based on Fe/N/C complex, developed by pyrolized of polyaniline /carbon nanotubes composites.

In conclusion, the catalytic activity of transition metal macrocyclic compounds towards ORR strongly depends on the individual transition metal center and the macrocyclic ligand, as well as the size of the π electron system. Compounds studied previously include a variety of metal centers and ligands. The transition metals used in macrocyclic catalysts include Fe, Co, Ni, and Cu, and the macrocyclic ligands include chelating atoms N_4, N_2, O_2, N_2S_2, O_4, and S_4. The conjugate π electron compounds usually include metal

phthalocyanine and porphyrin, as well as their derivatives. The activity of these compounds changes with respect to the central metal ions in the following order: Fe> Co > Ni > Cu. For a metal center, the chelating atoms of the macrocyclic ring can also change the ORR activity. For example, the active sequence of Fe complexes is as follows: $N_4 > N_2O_2 > N_2S_2 > O_4 \approx S_4$ (inactive); for Co centers: $N_2O_2 > N_4 > N_2S_2 > O_4 \approx S_4$; for Cu centers: $N_4 > O_4 > N_2O_2 > N_2S_1 > S_4$ (inactive); and for Ni centers: $O_4 > N_2O_2 > N_2S_2 > N_4$. With respect to these active sequences, recent research has mainly focused on Fe and Co centers, and for macrocyclic rings, on the N_4 system.[4] Therefore today, catalysts obtained from the pyrolysis of elemental precursors and where the metal is either Fe and/or Co are the most promising non-platinum electrocatalysts for oxygen reduction reaction.

2.2 Research Problem

Although, Pt and its alloys are known as the best efficient catalysts for activation of the strong oxygen–oxygen double bond,[5-6] their application is limited by the high cost and scarce reserve. To overcome this problem, low-cost, non-precious metal catalysts have attracted much attention as an alternative to Pt for a new generation of fuel cells and metal-air batteries,[32] As can be seen in the literature, among the non-precious catalysts studied, Fe–N–C catalysts have attracted much interest owing to their low-cost and facile preparation methods.[33] However, today's Fe–N–C catalysts still suffer from low activity and poor durability, especially for unpyrolysed Fe–N–C catalysts. The typical cycle life for unpyrolysed Fe–N–C catalysts is less than 100 cycles in either acidic or basic media.[7,34] It is still a great challenge to replace Pt-based catalysts by inexpensive Fe–N–C catalysts while maintaining similar performance in practical applications.

Since Fe and Co have been identified as the best central transition metals for the catalysts, the only variables left to play with are nitrogen and carbon sources. In that regard, porphyrins and phthalocyanines, are the precursors most widely used to prepare ORR catalysts. Metal macrocycle was first observed to facilitate ORR in fuel cells in 1964,[8] and were then thoroughly investigated as potential cathode catalyst in fuel cells and metal-air batteries.[35] To date, however, limited progress has been made in improving their electrocatalytic activity and durability. [36] In particular, macrocycle compounds have been known for a long time to suffer from severe degradation in fuel cell environments due to demetalation and/or degradation of iron phthalocyanine (FePc) by ORR intermediates.[37] Hence, scientists are exploring other alternatives in order to come up with high active and durable catalyst systems.

2.3 Vinazene

Considering the limitations regarding the existing macrocyclic, the need to search for new nitrogen containing compound becomes inevitable and this prompts the choice of vinazene. Vinazene is a derivative of imidazole rich in nitrogen content. Meanwhile imidazolic framework together with phenanthroline was used as nitrogen precursor by Prioietti et`al. [38] Hosogai reported for the first time the synthesis of vinazene without any report on its polymerization and its reactions,[39] Rasmussen et al.[40] however reported the improved synthesis of vinazene and its simple polymerization pathways. As shown in figure 2b below, its high nitrogen content, 39%, along with intrinsic stability of imidazole ring system, gives the polymer the potential for providing inhibition of flammability, higher softening temperatures, and greater char yields than any conventional materials. In

fact total gas evolution can be low and char yield and nitrogen retention are remarkably high, even in temperature as high as 900 ^{o}C, under nitrogen atmosphere as seen in figure 2a below.[40] The stoichiometric composition of the material, with high nitrogen content and low hydrogen content suggests their use as flame retardants, protective coatings and in specialty materials which demand high oxidation resistance.[40]

Furthermore, it is a very strong electron acceptor and as a result it has been used for solar cell applications.[41]

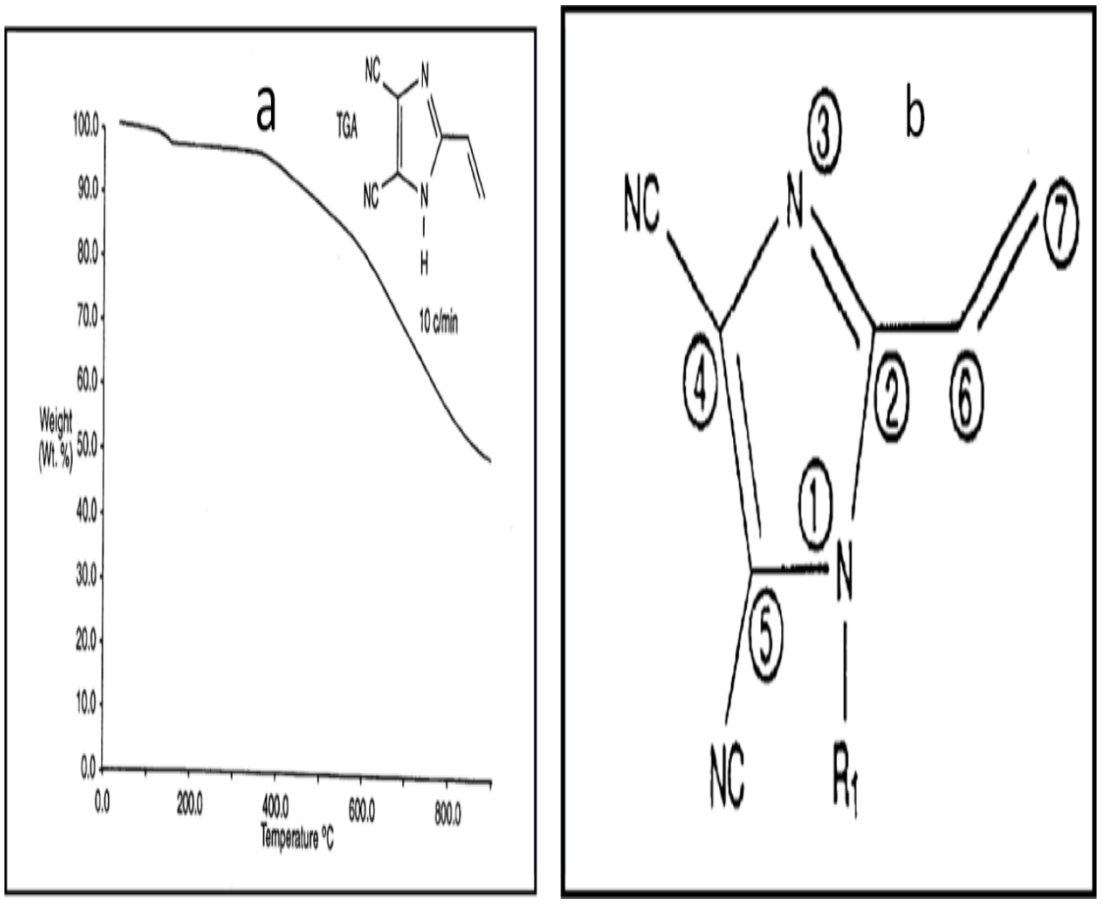

FIGURE 2: (A) THERMAL GRAVIMETRIC ANALYSIS OF VINAZENE.[42] (B) VINAZENE STRUCTURE.[40]

Drawing inspiration from good thermal stability and electronic properties of vinazene, we are demonstrating for the first time the possibility of using vinazene in developing ORR catalysts. Fe/N/C electrocatalyst based on vinazene/Fe modified carbon through simple and environmental friendly synthetic pathway was developed and showed remarkable ORR activity and cycling durability.

2.4 Research Objective

1. To understand the thermal behaviour of vinazene with and without carbon support.
2. To develop a Fe-N-C composite catalyst based on pyrolized vinazene-carbon composites as platinum-free for oxygen reduction reaction in fuel cells.
3. To enhance active sites in Fe-N-c catalysts (increase Nitrogen to Carbon ratio) for ORR activity.
4. To obtain a system that is chemically and electrochemically stable.
5. To obtain a high surface area of Fe-N-C catalyst modified carbon by using Vinazene.
6. Characterization of the synthesized catalyst using RAMAN, XRD, SEM-EDX and XPS to provide information about morphology and elemental analysis in order to highlight the active sites towards oxygen reduction reaction.
7. To evaluate electrochemical performance of the catalyst in acidic and basic media by voltamperometry and rotating disk electrode (RDE).

CHAPTER 3

METHODOLOGY

3.1 Materials

Vinazene was purchased from Vinazene Inc, USA. Ketjenblack EC-300 was obtained from AKZO Nobel, USA. Vulcan XC-72 purchased from Cabot, USA MilliQ UV-plus water (Millipore) was used throughout the experiments. Acetonitrile from JT Baker USA and Isopropyl alcohol (IPA) from Fisher Scientific were used as solvents. And Potassium hydroxide was purchased from Prolabo (BDH), France.

3.2 Catalyst Synthesis

The Fe-N-C was prepared by exploiting the solubility of vinazene in acetonitrile and isopropyl alcohol (IPA). After thorough impregnation of vinazene on kejtenblack in acetonitrile/IPA solution, iron precursor was added to complex on vinazene/carbon matrix followed by heat treatment in inert atmosphere to lead to Fe-N-C matrix.

In a typical synthesis, it involved dispersion of 200mg Ketjenblack carbon in a mixture of acetonitrile(ACN) and isopropyl alcohol (IPA) followed by sonication for 30min. Approximately 100 mg vinazene was then added to the mixture which is equivalent to ratio 1: 2 to the carbon and left under stirring for 48hrs in an enclosed system under room temperature to prevent solvent evaporation and allow proper impregnation of Vinazene into the carbon. 170mg of $FeCl_3.6H_2O$ (10% Fe) was added to the mixture and kept under stirring for another 24hrs under room temperature as well. The obtained mixture was then opened to allow solvent evaporation and formation of slurry while still stirring at room temperature. The resultant thick slurry was then vacuum dried at elevated temperature,

70^{o}C for 7hrs. The scheme below illustrated pathway to obtain Fe-N-C catalyst using vinazene.

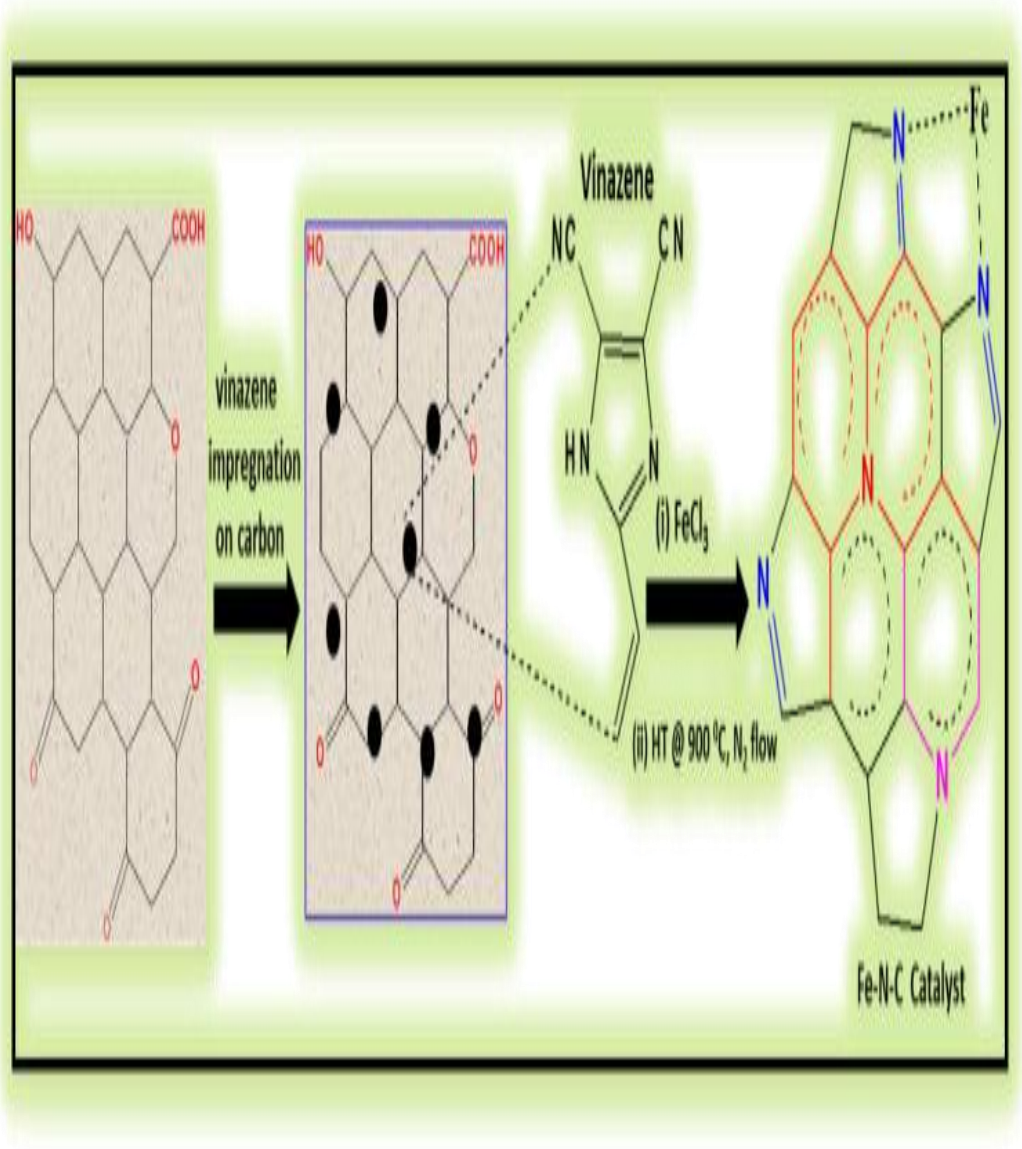

Scheme 2: Proposed synthetic pathway for the Fe-N-C catalyst.

3.3 Heat treatment

Heat treatment has been identified as crucial step to improve the activity of electrocatalysts, and in this regard, 900^{o}C has also been identified as optimum heat treatment temperature. In this case, the mixture obtained above is subjected to heat treatment as shown below

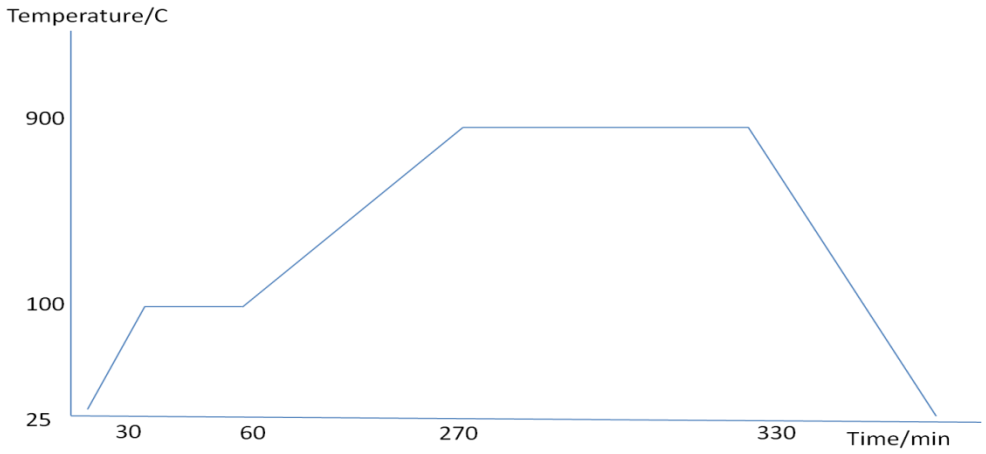

Figure 3: Schematic Diagram of Heat Treatment Process

As depicted in the figure above, the temperature is ramped from room temperature to 100 ^{o}C for 30min in inert atmosphere and held at 100 ^{o}C for another 30min. This is very important step as it reduces possible sources of oxygen and water from the system as oxygen source is known to consume carbon. After that, temperature was ramped to 900 ^{o}C at rate of 5 ^{o}C/min and held at this temperature for 60 min, while keeping nitrogen flow on. The system was then allowed to cool down.

The heat treatment could cause structural and surface change to the carbon support. These defects could as well be the hosts for the formation of pyrrolic, pyridinic and graphitic

nitrogen functions which are known to be the active sites for oxygen reduction reaction. It could also cause creation of pores due to degasification, such as evolution of Cl_2, CN, CO_2 and possibly CO.

Figure 4: Picture of High Temperature Furnace Used for the Heat Treatment

3.4 Characterization

In order to understand and give possible explanation for the observed performance of the developed catalyst, different spectroscopic techniques and surface area analyser, as well as electrochemical techniques have been employed.

3.4.1 Surface Area Analysis (BET)

BET surface area of both raw Carbon and heat treated catalysts will be calculated on Tristar Micromeritics sorptometer (ASAP 2020 surface Area and Porosity Analyzer) using liquid nitrogen as an adsorbant at (-176 ^{o}C) temperature. Prior to BET surface area determination, the samples will be degassed for 3hours at 350 ^{o}C to remove any presence of impurities.

3.4.2 Thermogravimetric Analysis

Thermal gravimetric analysis of raw carbon, vinazene and vinazene/carbon will be evaluated by STA 449F3- Jupiter made by Netzsch

3.4.3 Field Emmision Scanning Electron Microscope

TESCAN- LYRA 3 FESEM (manufactured in Czech Republic) will be used to examine the morphology of catalyst samples with energy dispersive X-ray spectrometer detector for elemental analysis.

3.4.4 Raman Spectroscopy

Raman spectroscopy technique (iHR320 with CCD detector, HORIBA, France) will be used at 532nm (less than 300mW, green laser) to observe D and G-bands of both raw carbon and catalyst, also to evaluate the degree of graphitization of Carbon nanostructures grown by ratio of intensity of G-band to D-band (I_g/I_d).

3.4.5 X-ray Diffraction (XRD)

X-ray diffraction (XRD) will be employed to evaluate the crystallinity and presence of active sites.

3.4.6 X-ray photoelectron spectroscopy (XPS)

X-ray photoelectron spectroscopy (XPS) will help us to evaluate the nature of nitrogen functionalities in the catalyst.

3.5 Electrode Preparation *and* Electrochemical Studies

3.5.1 Ink Preparation

For ORR activity measurements, approximately 5mg of the dried catalyst Fe-N-C/x was dispersed in a mixture of water and isopropanol alcohol (30%, v/v) and 37µl of 1.66 wt.% Nafion® (prepared from 5wt.%, Aldrich). The mixture was then ultrasonicated for 10–20min to obtain a uniform ink. Then, 16µl of the ink suspension were deposited on a pre-cleaned glassy carbon substrate (5 mm diameter, Pine Instruments) and allowed to dry. For higher loading of catalyst, the operation was repeated for several times to achieve the desired catalyst loadings.

3.5.2 Electrochemical Analysis

Ag–AgCl or SCE electrode (calibrated against reversible hydrogen electrode, RHE) and Pt mesh were used as a reference and counter electrode, respectively. The set up is shown in the fig 5 shown below. All the potentials reported in this paper are converted to RHE. Before testing ORR activity, each electrode was subjected to cycling in nitrogen saturated 0.1M $HClO_4$ and 0.1M KOH solutions until a stable CV was obtained (generally for 10–15 cycles between 0 and 1.2 V at 20 mV s^{-1}). ORR activity was evaluated in both oxygen saturated acidic (0.1 M $HClO_4$) and alkaline (0.1 M KOH) media using a rotating disk electrode (RDE) technique at rotation speed of 100, 400, 900 and 1600 rpm with scan rate of 5 mV s^{-1}. Catalysts durability was also investigated in oxygen saturated 0.1M

$HClO_4$ and 0.1 M KOH under potential cycling between 0.65 and 1.0 V for 15,000 cycles using square-wave signal of 5sec at each potential. During potential cycling test, ORR activity was evaluated in fresh electrolytes in a separate cell after every 5000 cycles. The ORR activity of catalysts was also measured in 0.1M $HClO_4$ containing 0.1M methanol to evaluate its methanol tolerance. All the currents are normalized to the geometric area of the electrodes.

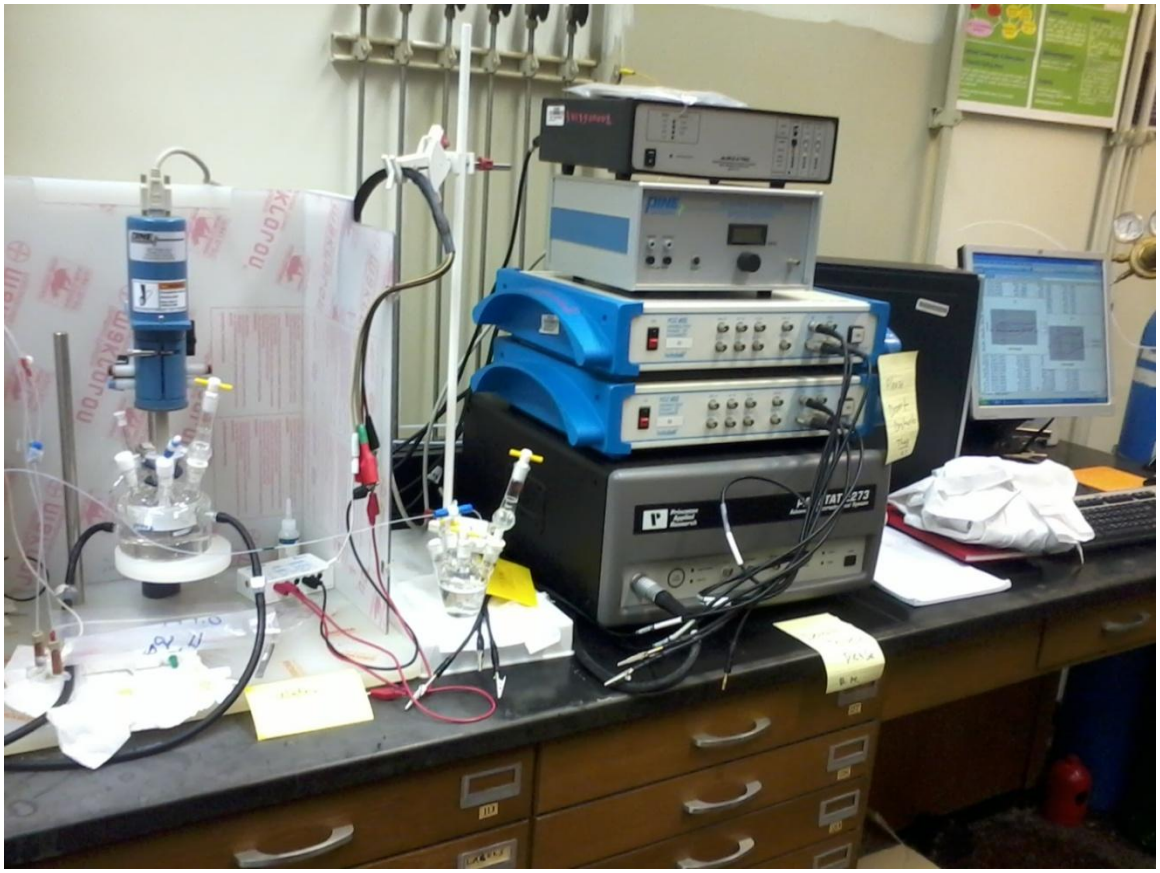

Figure 5: Experimental Set-up for Electrochemical Analysis

3.5.3 Koutechy-Levich

The number of electron involved per mole of oxygen was calculated by Koutechy-Levich principle according to the equations below:

$$1/j = 1/j_k + 1/j_{lim}$$

$$= 1/nFCo2Ko2\Gamma \quad + \quad 1/0.62nFC_{O2}D_{O2}^{2/3}V^{1/6}\omega^{1/2}$$

where n represents the overall electron transfer number per mole of oxygen, F is the Faraday constant with the value of 96485 C mol^{-1}, D_{O2} is the diffusion coefficient of O_2 in 0.1 M KOH ($1.9 \times 10^{-5} cm^2 s^{-1}$), vis the kinetic viscosity (0.01 $cm^2 s^{-1}$),and C_{O2} is the bulk concentration of O_2 (1.2×10^{-6} mol cm^{-3}). The constant 0.2 is adopted when the rotation speed is expressed in rpm in alkaline aqueous solution.

CHAPTER 4

RESULT AND DISCUSSION

As stated in the previous chapter, spectroscopy characterizations, thermal stability analysis and surface area and porosity analysis were conducted on the synthesized catalysts to give genuine possible explanations for the observed excellent performance of the catalysts.

4.1 Thermal Gravimetric Analysis

Thermogravimetric analysis or thermal gravimetric analysis (TGA) is a method of thermal analysis in which changes in physical and chemical properties of materials are measured as a function of increasing temperature (with constant heating rate), or as a function of time (with constant temperature and/or constant mass loss). TGA is commonly used to determine selected characteristics of materials that exhibit either mass loss or gain due to decomposition, oxidation, or loss of volatiles (such as moisture). Common applications of TGA are (1) materials characterization through analysis of characteristic decomposition patterns, (2) studies of degradation mechanisms and reaction kinetics, (3) determination of organic content in a sample, and (4) determination of inorganic (e.g. ash) content in a sample, which may be useful for corroborating predicted material structures or simply used as a chemical analysis. Since we have interest in stability of the particular elemental compositions of the composite after heat treatment which will likely determine number of active sites, thermal stability of the catalyst was

tested to have understanding of its possible behavior during heat treatment as shown in the figure below.

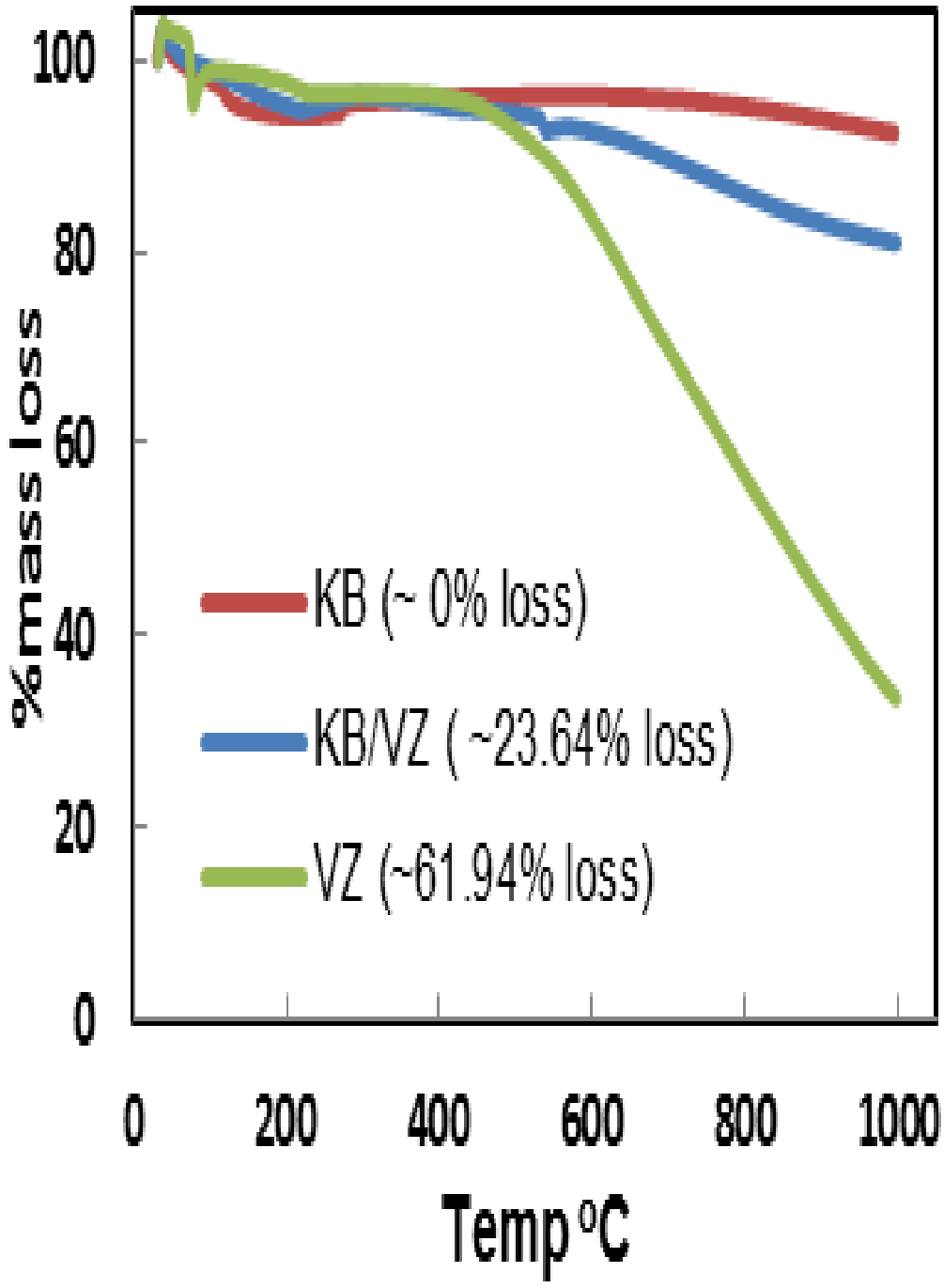

Figure 6: TGA Result of VZ-KB Composite.

As evidenced from thermo gravimetric data, which show weight loss of 23.64% (with carbon support) and 61.94% (without carbon support) (Fig. 6). It is likely that the loss in the presence of carbon support is due to the decomposition of vinazene molecule by the release of side groups and subsequent fusion of the aromatic ring on the carbon surface. This also corroborates what was revealed by XPS.

4.2 Raman Spectroscopy

Raman spectroscopy provides information needed to elucidate the morphological changes done to the carbon support after impregnation and complexation of Fe/vinazene into the carbon matrix followed by heat treatment. This is always used to explain the amount of defect caused to the carbon support by evaluating the intensity ratio of Defect-band (D-band) to the Graphitic –band (G-band). For many applications in this context, the aim is to dope the carbon structure with molecule(s) or atom(s) of interest, therefore the extent of doping can be evaluated by the degree of defect. The so-called G-line is a characteristic feature of the graphitic layers which corresponds to the tangential vibration of Carbon atoms. The D-line mode is a typical sign for defective graphitic structure.[43] The ratio of these two peaks intensities gives a measure of the degree of defect created on carbon surface. As a result, this spectroscopic technique was conducted on the raw carbon and synthesized catalysts as shown in the figure and table below.

The table and fig below compare the peak responses of the catalyst and raw carbon. The peaks revealed from the figure above centered around 1334cm^{-1} and 1595cm^{-1} are designated as D-band and G-band respectively.[31]

As can be seen from the Raman spectra of the two catalysts, the I_D/I_G ratio (1.2) of the

synthesized catalyst based on KB is almost same as that for the raw carbon (KB).

Table 1: The D/G ratios of the raw carbon and catalysts obtained from the RAMAN spectra.

Material	D-band	G-band	Ratio
HT-Fe-N-KB	2245.46 cm^{-1}	2000.63	1.12
HT-Fe-N-Vul	1590 cm^{-1}	1793.65 cm^{-1}	0.7635
Kejtenblack	2258	1877.86	1.2
Vulcan	1550cm^{-1}	1552cm^{-1}	0.9978

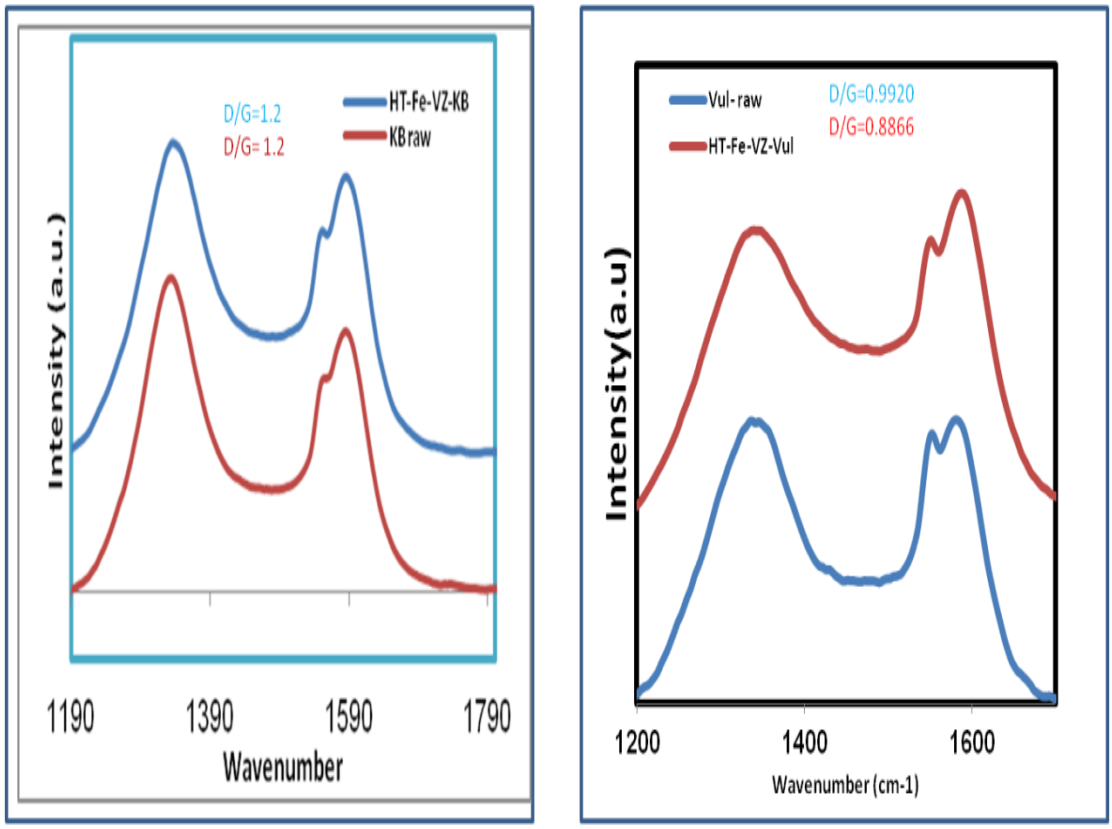

Figure 7: RAMAN spectra of the raw carbon and catalysts

While the I_D/I_G ratio (1.2) of the synthesized catalyst based on Vulcan is slightly different from that of the I_D/I_G ratio of the raw carbon. Generally, for highly crystalline carbon, the ratio I_D/I_G is around 0.1, while it is close to unity in the case of disordered or polycrystalline carbon.[44] This clearly indicates that our catalyst is in polycrystalline form and the heat treatment at 900^{o}C presumably did not alter much the structure of the carbon support in the case of catalyst based on kejtenblack(KB), while there is slight improvement in graphitic structure of the catalyst based on Vulcan(Vul) after the heat treatment. This may be due to low defect created on carbon surface.

4.3 X-Ray Diffraction

Analysis of the diffraction pattern allows the identification of phases within a given sample. It may be possible to quantify each phase present, the crystallinity of a sample, the crystal structures and their lattice parameters, crystallite size and strain, all information that can be vital in material characterization and quality control. The properties of a material can often be linked back to the arrangement of atoms in its crystal structure. X-ray diffraction is a non-destructive analytical technique. This technique was used to examine the structure of the synthesized catalysts. The catalysts synthesized during this work show broad diffraction peaks at 25-26^0 which have been attributed to the (002) carbon in graphitic form. The retention of these strong intensities of the peaks after heat treatment at 900 ^{0}C further establishes formation of nitrogen-doped carbon without necessarily sacrificing the graphitic form which is in agreement with Raman data, especially for the catalyst based on KB.

The figure 8 below shows the diffraction patterns of the two catalysts.

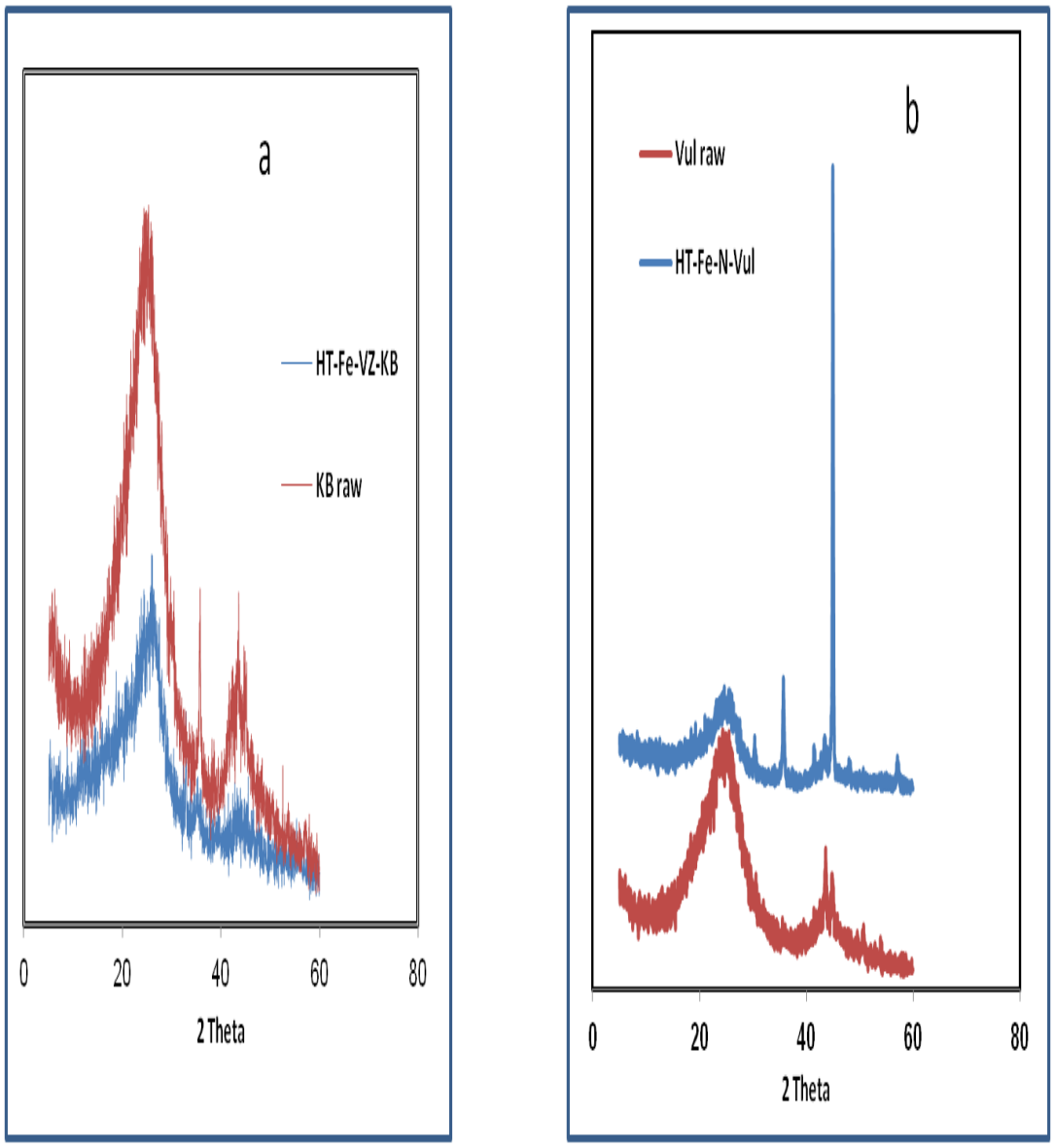

Figure 8: XRD patterns of the synthesized catalysts (a) Fe-N-C/KB (b) Fe-N-C/Vul

Moreover, the diffraction peaks centered at 43-45^0 in the two catalysts can be attributed to Fe-N functionalities and Fe nanoparticles. This particular peak is much more

pronounced for the catalyst based on Vulcan which may denote more formation of some Fe particles.

4.4 Field Emission Scanning Electron Microscope

High-end–field emission scanning electron microscope (FESEM, Tescan-Lyra-3) was used to provide images of the synthesized catalysts. A scanning electron microscope (SEM) is a type of electron microscope that produces images of a sample by scanning it with a focused beam of electrons. The electrons interact with atoms in the sample, producing various signals that can be detected and that contain information about the sample's surface topography and composition. The electron beam is generally scanned in a raster scan pattern, and the beam's position is combined with the detected signal to produce an image. SEM can achieve resolution better than 1 nanometer. Specimens can be observed in high vacuum, in low vacuum, and (in environmental SEM) in wet conditions.

The most common mode of detection is by secondary electrons emitted by atoms excited by the electron beam. The number of secondary electrons is a function of the angle between the surface and the beam. On a flat surface, the plume of secondary electrons is mostly contained by the sample, but on a tilted surface, the plume is partially exposed and more electrons are emitted. By scanning the sample and detecting the secondary electrons, an image displaying the tilt of the surface is created. The types of signals produced by a SEM include secondary electrons (SE), back-scattered electrons (BSE), characteristic X-rays, light (cathodoluminescence) (CL), specimen

current and transmitted electrons. Secondary electron detectors are standard equipment in all SEMs, generally it is rare that a single machine would have detectors for all possible signals. The signals result from interactions of the electron beam with atoms at or near the surface of the sample. In the most common or standard detection mode, secondary electron imaging or SEI, the SEM can produce very high-resolution images of a sample surface, revealing details less than 1 nm in size. To reveal the topography and composition of our synthesized catalysts, High Field Scanning Electron Microscope was used to characterize the catalysts as shown in the figure below. The images clearly reveal porous structure for the two catalysts with particle sizes ranging between 15 -20nm for Fe-N-C/KB while the particle sizes for the Fe-N-C/Vul ranges between 40-50nm. Such porous structure is beneficial because it plays a significant role in managing both reactants and products during the electrode reactions. It is also very crucial for enhanced electrode performance, particularly in the case of M-N-C catalysts (where M is a non-noble metal), since higher the porosity, more available are the active sites for ORR.[45] It can be seen from the figure above that synthesized catalyst based on KB is more porous and contain smaller particles than the catalyst based on Vul which is also corroborated what was revealed by BET. This is indeed may be responsible for better activity displayed by Fe-N-C/KB.

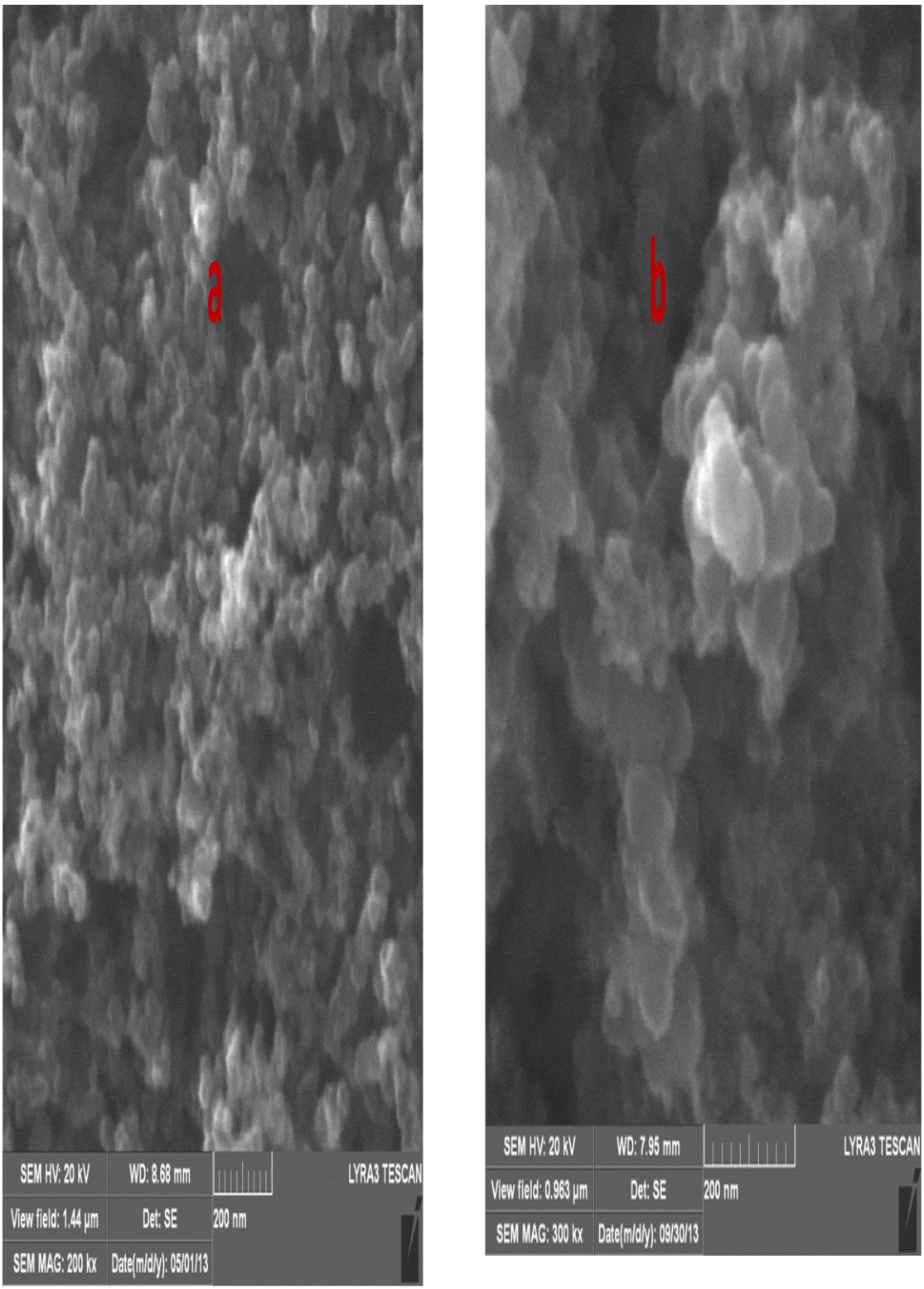

Figure 9: SEM images of the synthesized catalysts with the same magnification of 200nm bar (a) Fe-N-C/KB (b) Fe-N-C/Vul.

4.5 Energy Dispersive X-Ray

Energy-dispersive X-ray spectroscopy (EDS, EDX, or XEDS), sometimes called energy dispersive X-ray analysis (EDXA) or energy dispersive X-ray microanalysis (EDXMA), is an analytical technique used for the elemental analysis or chemical characterization of a sample. It relies on an interaction of some source of X-ray excitation and a sample. Its characterization capabilities are due in large part to the fundamental principle that each element has a unique atomic structure allowing unique set of peaks on its X-ray spectrum. To stimulate the emission of characteristic X-rays from a specimen, a high-energy beam of charged particles such as electrons or protons (see PIXE), or a beam of X-rays, is focused into the sample being studied. At rest, an atom within the sample contains ground state (or unexcited) electrons in discrete energy levels or electron shells bound to the nucleus. The incident beam may excite an electron in an inner shell, ejecting it from the shell while creating an electron hole where the electron was. An electron from an outer, higher-energy shell then fills the hole, and the difference in energy between the higher-energy shell and the lower energy shell may be released in the form of an X-ray. The number and energy of the X-rays emitted from a specimen can be measured by an energy-dispersive spectrometer. As the energy of the X-rays is characteristic of the difference in energy between the two shells, and of the atomic structure of the element from which they were emitted, this allows the elemental composition of the specimen to be measured.

Processing option : All elements analysed (Normalised)

Spectrum	In stats.	C	N	S	Cl	Fe	Total
Spectrum 1	Yes	90.53	7.74	0.28	0.26	1.19	100.00
Spectrum 2	Yes	89.68	8.20	0.34	0.29	1.48	100.00
Spectrum 3	Yes	84.25	13.43	0.33	0.31	1.68	100.00
Spectrum 4	Yes	89.83	7.82	0.31	0.32	1.73	100.00
Spectrum 5	Yes	90.74	6.76	0.35	0.20	1.96	100.00
Spectrum 6	Yes	84.28	12.42	0.40	0.31	2.59	100.00
Spectrum 7	Yes	87.00	9.88	0.35	0.32	2.45	100.00
Spectrum 8	Yes	90.91	6.63	0.31	0.25	1.90	100.00
Mean		88.40	9.11	0.33	0.28	1.87	100.00
Std. deviation		2.83	2.57	0.04	0.04	0.47	
Max.		90.91	13.43	0.40	0.32	2.59	
Min.		84.25	6.63	0.28	0.20	1.19	

a

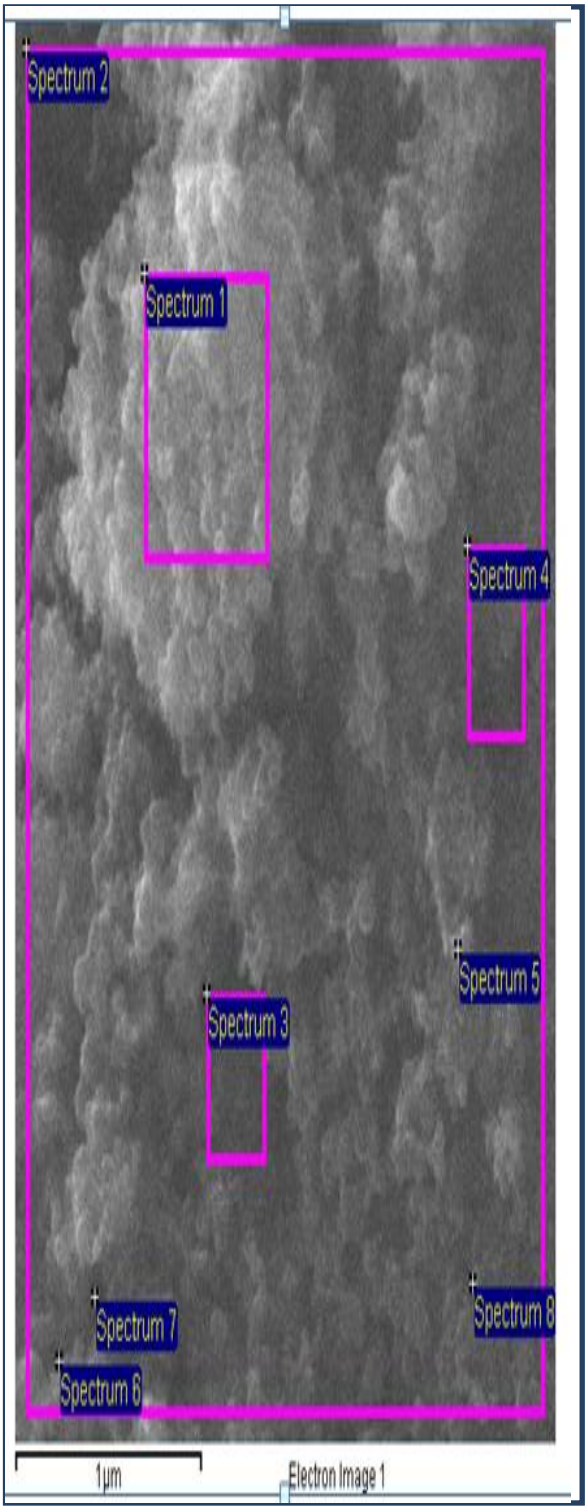

b

Spectrum	In stats.	C	N	O	Cl	Cr	Fe	Total
Spectrum 1	Yes	43.97	3.19	35.83	0.38	10.23	6.40	100.00
Spectrum 2	Yes	34.98	2.23	43.30	0.37	11.06	8.05	100.00
Spectrum 3	Yes	87.19	10.41		1.53		0.86	100.00
Spectrum 4	Yes	86.11	11.59		1.57		0.73	100.00
Spectrum 5	Yes	89.73	7.77		1.71		0.79	100.00
Max.		89.73	11.59	43.30	1.71	11.06	8.05	
Min.		34.98	2.23	35.83	0.37	10.23	0.73	

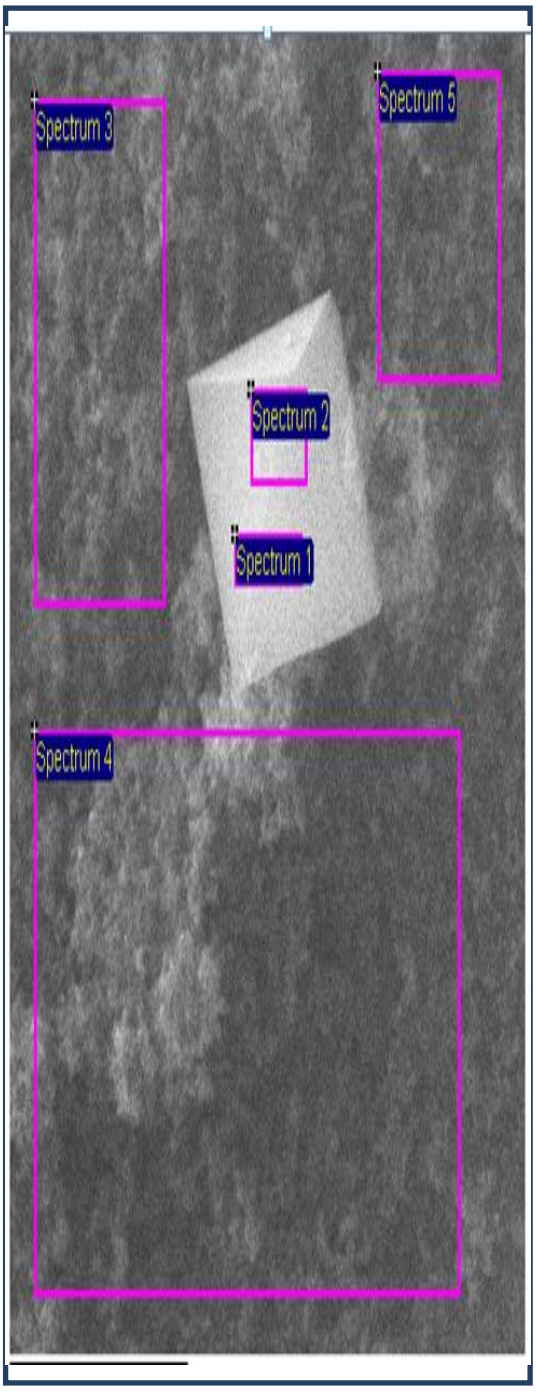

Figure 10: EDX tables for the synthesized catalysts (a) Fe-N-C/Vul (b) Fe-N-C/KB

Based on the figures above, we can summarize average composition of each element in the catalysts and nitrogen/carbon ratio as shown in the table below.

Table 2: Summary of average percent by weight of element in each catalyst

Catalysts	C	N	O	Fe	N/C
Fe-N-C/KB	68.396	7.038	15.826	3.366	0.103
Fe-N-C/Vul	88.4	9.11	0.23	1.87	0.103

As can be seen from the results above, each catalyst contain an appreciable percentage of nitrogen compared to what has been reported.[31] This may likely translate to more active sites that are responsible for better ORR activity. This also corroborates what was revealed in thermal gravimetric analysis where it was observed that vinazene molecule has better thermal stability especially when grafted on carbon support.

4.6 X-Ray Photoelectron Spectroscopy

X-ray photoelectron spectroscopy (XPS) is a surface-sensitive quantitative spectroscopic technique that measures the elemental composition at the parts per thousand ranges, empirical formula, chemical and electronic state of the elements that exist within a material. XPS spectra are obtained by irradiating a material with a beam of X-rays while simultaneously measuring the kinetic energy and number of electrons that escape from the top 0 to 10 nm of the material being analyzed. XPS requires high vacuum ($P \sim 10^{-8}$ millibar) or ultra-high vacuum (UHV; $P < 10^{-9}$ millibar)

conditions, although a current area of development is ambient-pressure XPS, in which samples are analyzed at pressures of a few tens of millibar. In this context, in an attempt to understand actual oxidation state of the active site i.e Fe/N/C, XPS measurements were carried out to examine the changes in surface of carbon as result of chemical and heat treatments.

As can be seen in the figure below this is almost similar to what was revealed by EDX. Meanwhile, it has been found in the literature that different types of nitrogen coordinations such as pyridinic, pyrrolic and graphitic in the carbon framework are responsible for creating different functionalities on carbon.

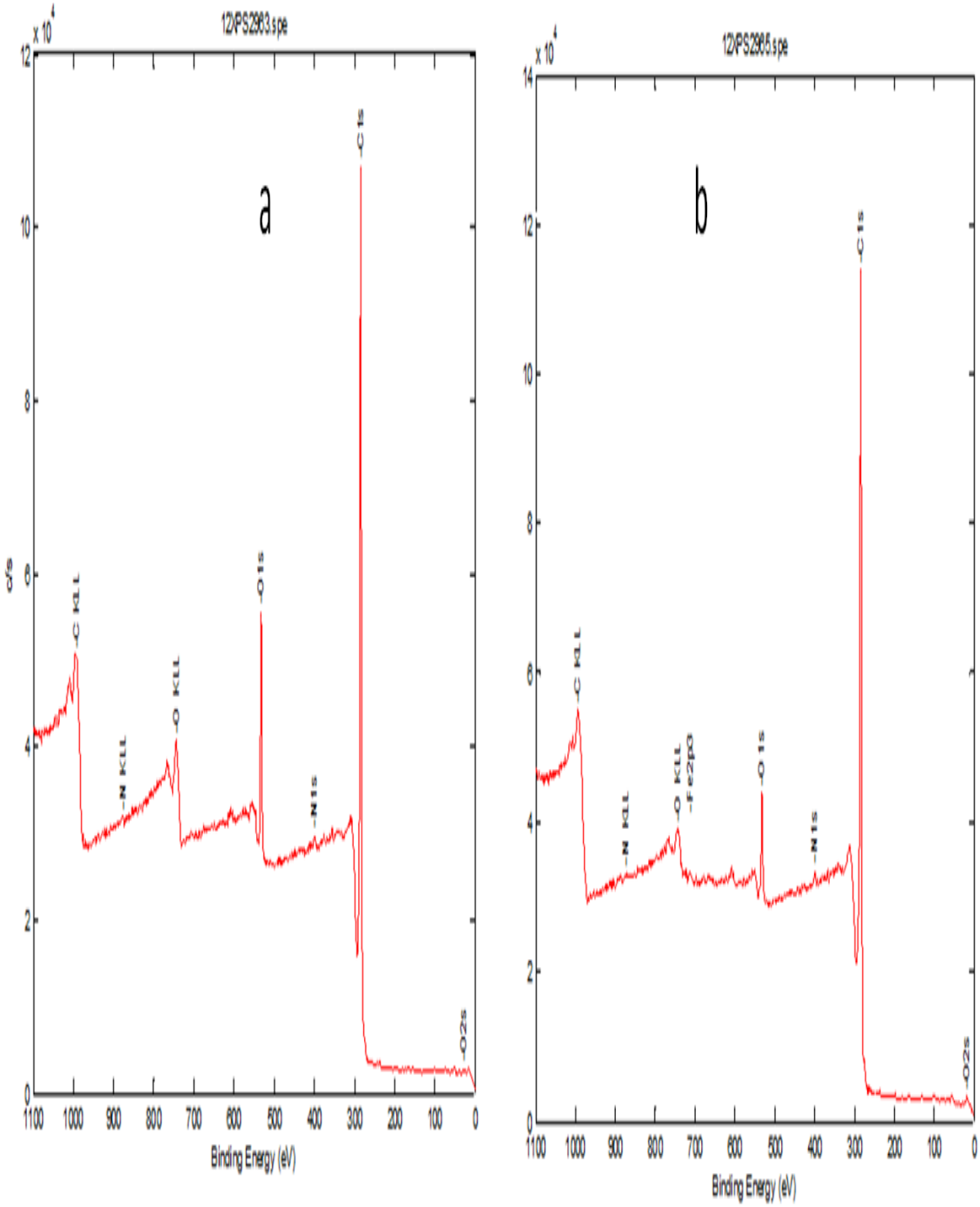

Figure 11: XPS Convulated spetra of (a) Fe-N-C/Ketjenblack (b)Fe-N-C/Vulcan

Therefore, the nature of nitrogen functionalities was also investigated as revealed in the figure below.

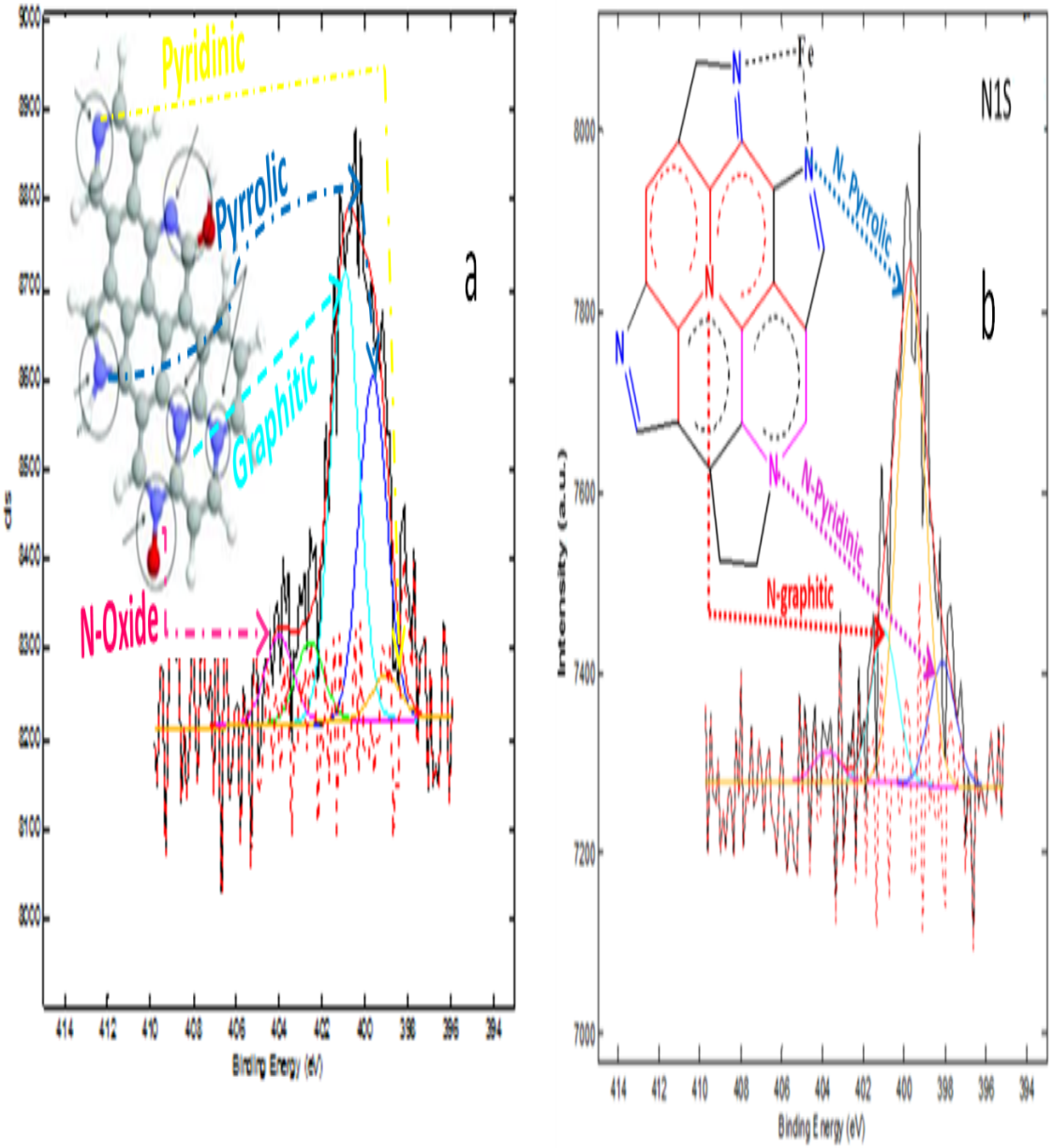

Figure 12: XPS Deconvoluted Peaks of N1s of (a)Fe-N-C/Vulcan (b) Fe-N-C/KB

As shown in Figure 12b, three different nitrogen bonding environments were revealed. The binding energy values of 398.13, 399.65, and 400.98 eV were identified as pyrridinic (15.05%), pyrrolic (65.71%), and graphitic (18.47%) nitrogen, respectively. As expected, due to the pyrrolic structure of the precursor vinazene, the synthesized (Fe-N-C) catalyst retained a high percentage of pyrrolic nitrogen functionality. This is also evidenced from the thermogravimetric data, which show weight loss of 23.64% (with carbon support) and 61.94% (without carbon support) (Figure 6). It is likely that the loss in the presence of carbon support is due to the decomposition of vinazene molecule by the release of cyanide groups and subsequent fusion of the aromatic ring on the carbon surface.

Recent studies have suggested that higher amount of pyrrolic nitrogen might be responsible for improved catalytic activities towards ORR.[19,22] However, we find this claim contradictory to the generally accepted fact that graphitic and not pyrrolic N is predominantly responsible for the excellent ORR activity.[31,46] So, one can associate such contradiction in catalytic activity of M-N-C with working condition, in particular type of electrolyte used for ORR evaluation. It should be pointed out, however, that in an acidic electrolyte, a catalyst rich in graphitic nitrogen is more preferred since the latter is more stable (not prone to protonation) than any other nitrogen functionalities. On the other hand, pyrrolic and pyridinic nitrogen and their metal-complexed functionalities could be more stable and do not undergo hydrolysis in an alkaline medium. This could be the reason for the observation of a Pt-like behavior of our Fe-N-C catalyst that is rich in pyrrolic nitrogen as revealed by XPS.

On the other hand, figure 12a revealed five different nitrogen environments. The binding energy values of 399.0, 399.61, 400.93, 402.56 and 404.01eV were identified as

pyrridinic (4.85%), pyrrolic (33.67%), graphitic (44.13%), protonated pyrrole (8.28%) and N-oxide nitrogen, respectively.

Two predominant nitrogen-doping types in this catalyst are graphitic nitrogen and pyrrolic nitrogen. The pyrrolic nitrogen represents nitrogen atoms doped at the edges of the pyrrolic carbon layers, and the graphitic nitrogen is denoted as the one doped inside the graphitic carbon plane. This suggests that the nitrogen atoms were successfully incorporated into the carbon structures and replaced carbon atoms located at the edges and inside of the graphitic carbon layers. As reported, the graphitic nitrogen plays a crucial role in oxygen reduction.

4.7 Surface Area Analysis

BET analysis provides precise specific surface area evaluation of materials by nitrogen multilayer adsorption measured as a function of relative pressure using a fully automated analyser. The technique encompasses external area and pore area evaluations to determine the total specific surface area in m^2/g yielding important information in studying the effects of surface porosity and particle size in many applications. In this context, surface area of raw carbons and synthesized catalysts were analyzed as given below**.**

Table 3: Surface Area result of the raw carbon and synthesized catalysts

Raw Carbon	Surface Area m^2/g	Catalyst	Surface Area m^2/g
Kejtenblack	803.247	Fe-N-C/KB	672.589
Vulcan	254	Fe-N-C/Vul	241.6889

The above table compares the surface area of the synthesized catalysts. The catalyst based on KB has higher surface area than the catalyst based on Vul. As can be seen from the result shown above, the large surface area and porosity of the catalysts may as well contribute to better performance, displayed by the catalysts. Though synthesized catalyst is somewhat lower in surface area compared to the raw carbon, this may be as a result of heat treatment and formation of Fe/N on the carbon support and thereby blocking some of the pores. However it is expected that the surface area of the synthesized catalyst will increase as a result of degasification of Cl_2 during heat treatment, but it is assumed that the degasification process is suppressed by the sintering process.

4.8 Electrochemical Analysis

The electrochemical behavior of the obtained catalysts which involve their activities, stability, and methanol tolerance were studied using thin film rotating disk electrode technique. As shown in the Figure 5, a typical set-up of three-electrode electrochemical cell was used for the analysis.

4.8.1 Electrode Preparation

The glassy carbon (5 mm diameter, Pine Instruments) was pre-cleaned using alumina and isopropanol with the support of sonication. The prepared ink according to the procedure mentioned in the methodology was then loaded onto the pre-cleaned electrode using

micropipette at rate of 16µl per loading. For higher loading, the operation was repeated until desired loading was achieved.

4.8.2 Effect of Carbon

Prior to oxygen reduction reaction measurements, each electrode (catalyst loading 0.6mg/cm^2) was potential cycled in nitrogen saturated 0.1M$HClO_4$ and 0.1MKOH for 15-20 cycles at 20mV/s until a stabilized cyclic Voltammogram (CV) was attained. Figure 13 shows a capacitive envelope between 0 and 1.2V/RHE with a pair of wide redox peaks which are almost symmetrical at 0.8V/RHE in alkaline medium. However, redox peaks become less visible because of large capacitive charge, especially for the catalyst, Fe-N-C/KB. Basically, the redox peaks that correspond to couple Fe^{II}/Fe^{III} is completely masked by the capacitive current. However, in acidic medium, the redox system is more visible as shown in Figure 14.

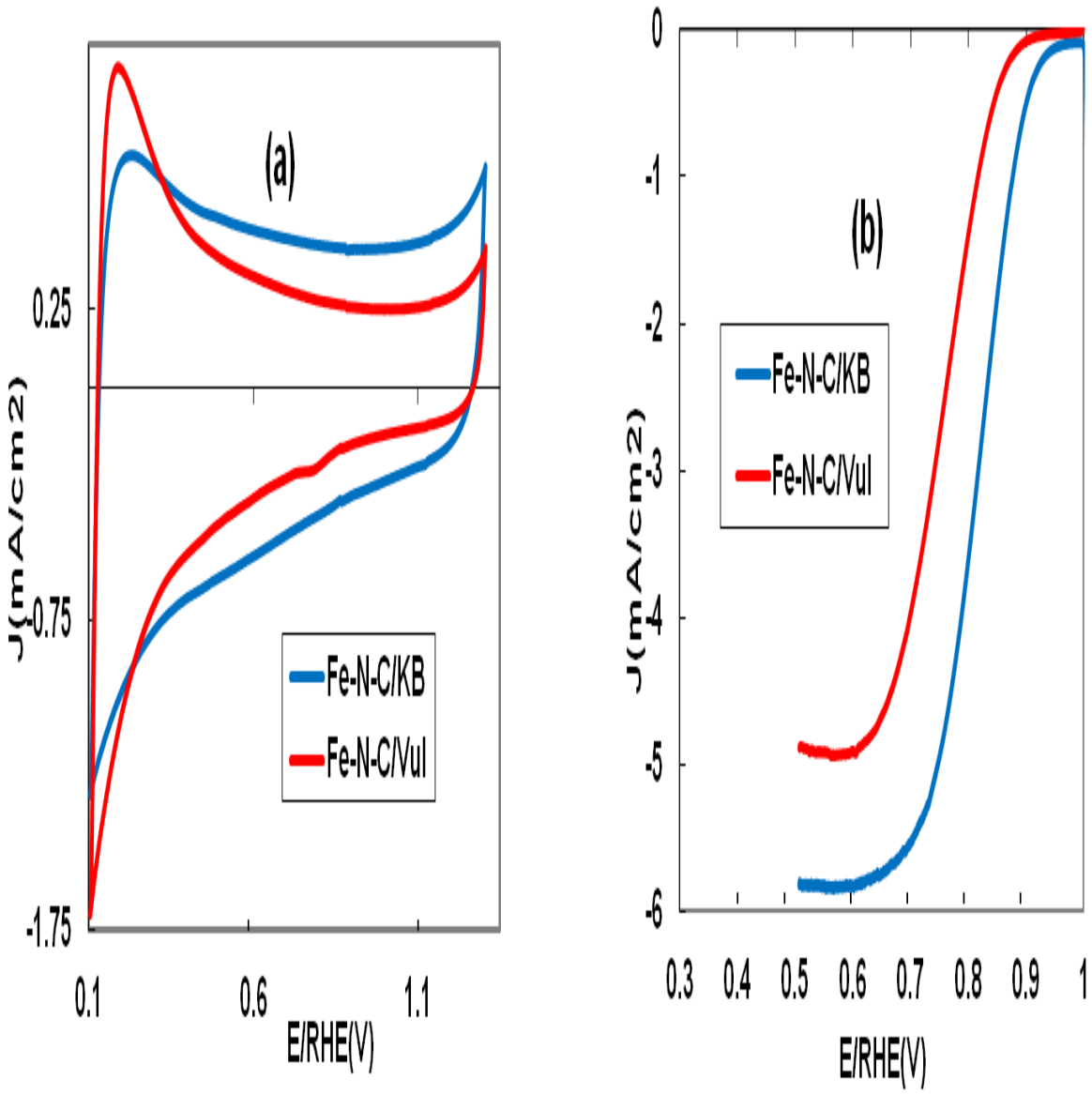

Figure13:(a) Cyclic Voltammetry in N2 saturated 0.1KOH of Fe-N-C/KB (blue) and Fe-N-C/Vul (red) (b) Linear Voltammetry in O_2 saturated 0.1KOH of Fe-N-C/KB (blue) and Fe-N-C/Vul (red)C/KB(blue)

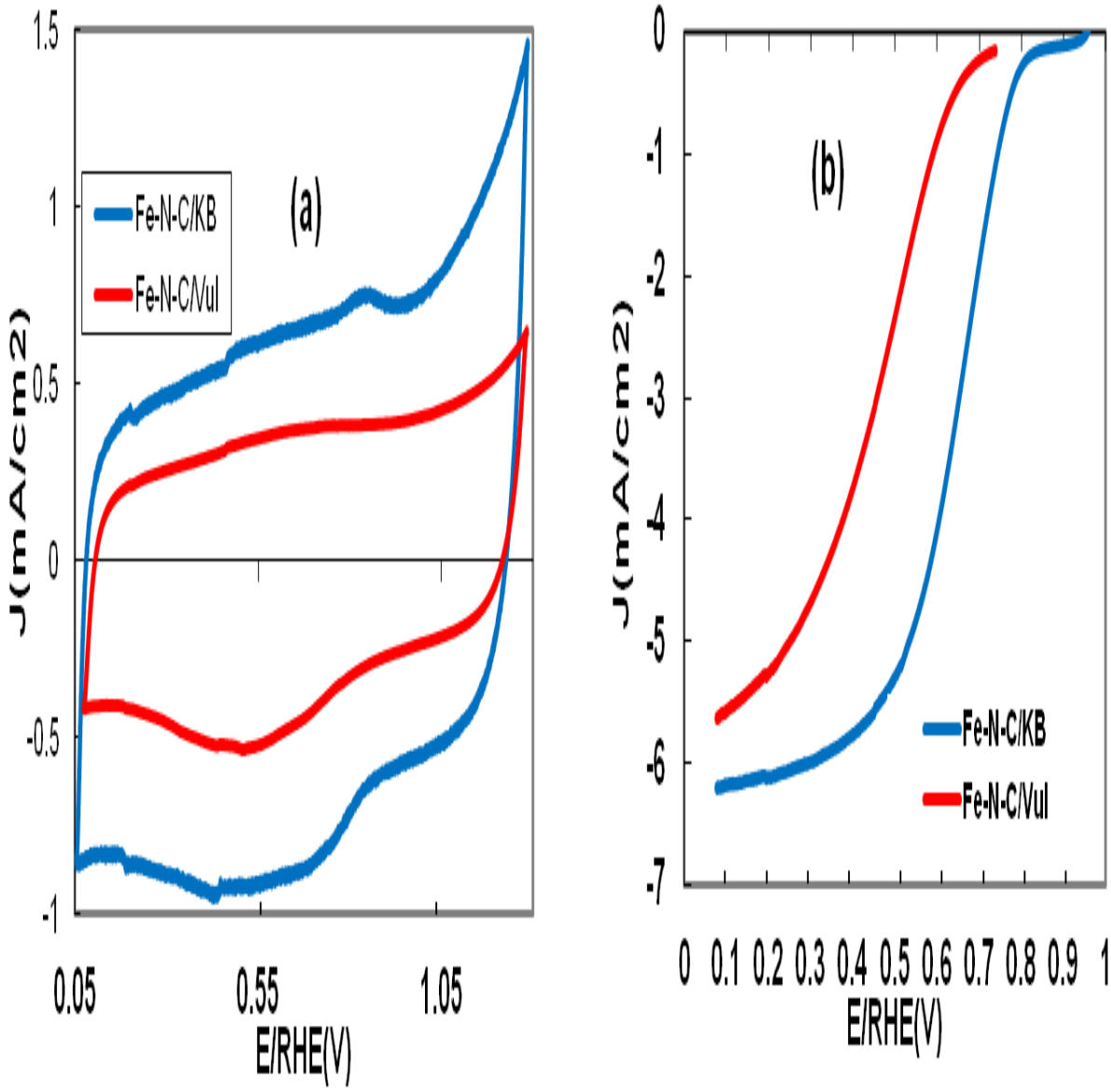

Figure 14:(a) Cyclic Voltammetry in N2 saturated 0.1HClO4 of Fe-N-C/KB (blue) and Fe-N-C/Vul (red) (b) Linear Voltammetry in O_2 saturated 0.1 $HClO_4$ of Fe-N-C/KB (blue) and Fe-N-C/Vul (red)C/KB(blue)

Table 4: Summary of onset and half wave potentials in 0.1M$HClO_4$ and 0.1MKOH

KOH(E/RHE(V))			$HClO_4$(E/RHE(V))	
Catalyst	E_1	$E_{1/2}$	E_1	$E_{1/2}$
Fe-N-C/Vul	0.9	0.755	0.80	0.467
Fe-N-C/KB	0.98	0.817	0.88	0.651

It is observed from the figures and table above that the catalyst Fe-N-C/KB has better activity than Fe-N-C/Vul, both in alkaline and acidic media. This can be noticed in the onset and half wave potentials values for the two catalysts. This trend may partially be due to large surface area possessed by Fe-N-C/KB as revealed by surface area analysis (BET area) which is also corroborated by higher capacitive envelop observed in cyclic voltammetry as shown above. In addition to that, catalysts also have different N-functionalities composition ratio as demonstrated by XPS results. It is important to note that there are three factors that govern the activity of this type of catalysts; (i) surface area, (ii) nitrogen content, and (iii) type of nitrogen.[31]

4.8.3 Effect of Catalyst Loading

The oxygen reduction activities of the two catalysts were evaluated in an oxygen saturated 0.1M$HClO_4$ and 0.1MKOH solutions with catalyst loadings of 0.2mg/cm^2, 0.4mg/cm^2 and 0.6mg/cm^2. The polarization curves obtained are shown in figure 15 in both acidic and alkaline media. It can be seen that the current densities of the two

catalysts in both kinetics and diffusion regimes increase with increasing the loading from 0.2mg/cm^2 to 0.6mg/cm^2. This may likely mean that number of electron transfer may depend on the loading and that 0.6mg/cm^2 may possibly support 4-electrons transfer because there are more active sites for oxygen and peroxide reduction. Such results are in good agreement with those reported for conventional catalysts, including Pt/C. Meanwhile, it is observed that the trend is not well respected for Fe-N-C/Vul in 0.1MKOH at low loading and especially if we take in consideration the limiting current. However, in the kinetic region the trend is more or less respected up to loading of 0.4 mg/cm2. At higher loading, no significant change in overvoltage of ORR (Fig. 15d) was observed. Electrode responses at 0.4mg/cm^2 and 0.6mg/cm^2 of the same catalyst have overlapped current densities in the kinetic region. This may translate to the fact that the optimum loading for Fe-N-C/Vul is 0.4mg/ cm^2 in alkaline medium,. Contrarily, in acidic medium both catalysts have shown that increase in loading led to a significant improvement in ORR activity in kinetic as well as limiting currents (Fig 16b and d).

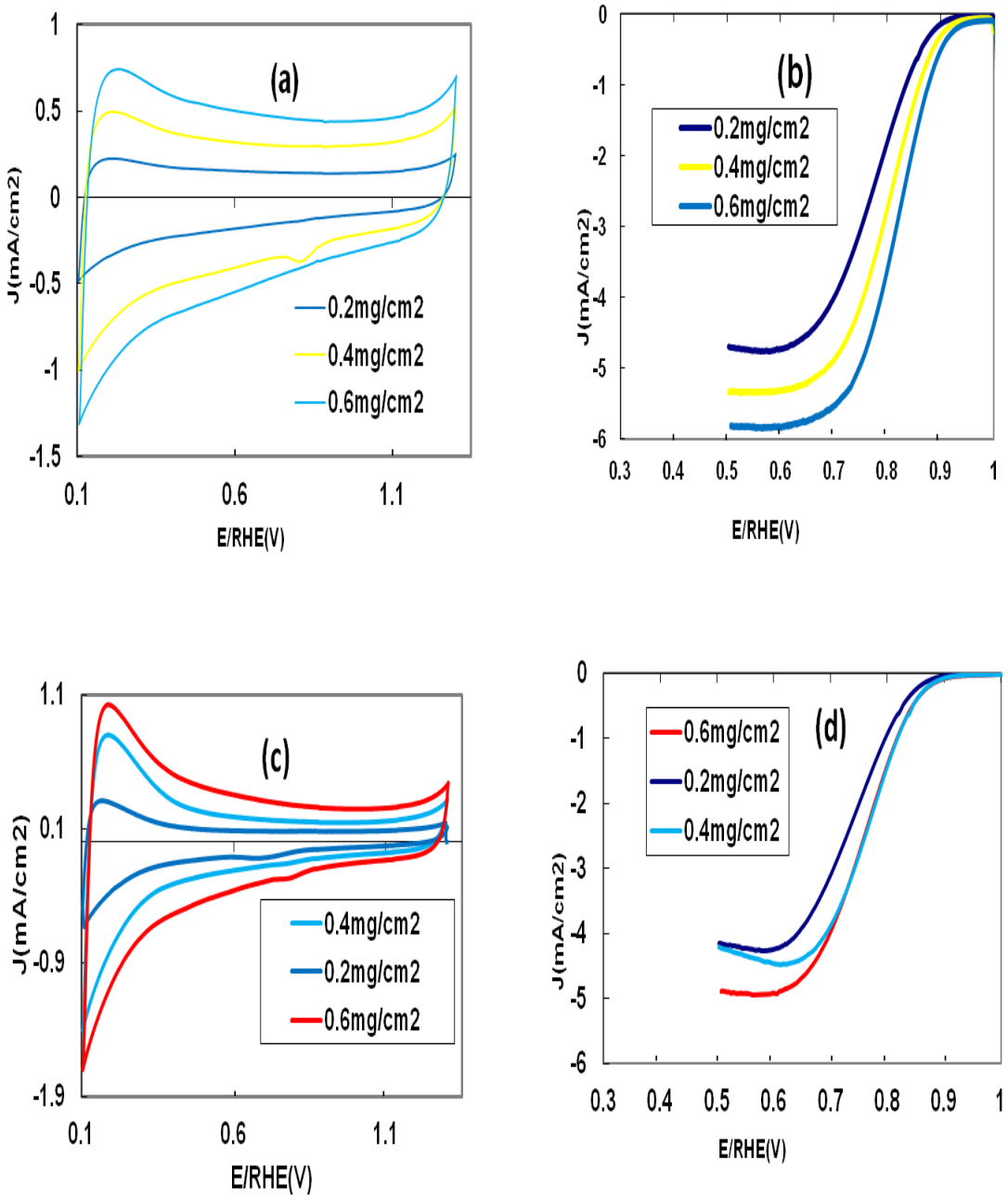

Figure 15: Catalyst loading effect in 0.1MKOH in: N_2 saturated (a)Fe-N-C/KB (c) Fe-N-C/Vul and, O_2 saturated (b) Fe-N-C/KB (d) Fe-N-C/Vul

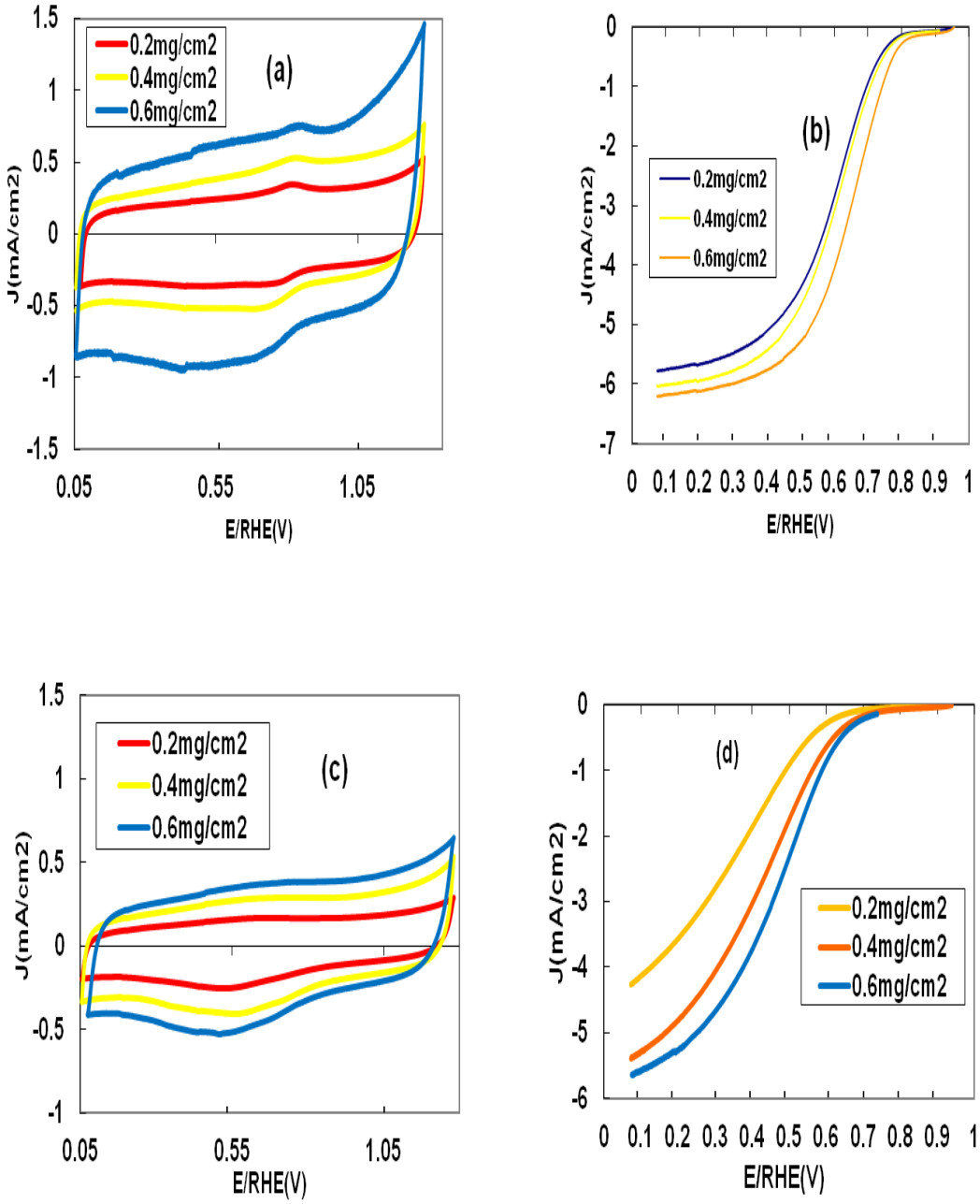

Figure 16: Catalyst loading effect in 0.1MHClO$_4$ in: N_2 saturated (a)Fe-N-C/KB (c) Fe-N-C/Vul and, O_2 saturated (b) Fe-N-C/KB (d) Fe-N-C/Vul

From electrode response, one can conclude that Fe-N-C/KB has the highest activity as compared to that of Fe-N-C/Vul. Noting that the two catalysts have different N-functionalities and surface area which may define their catalytic behaviors.

4.8.4 Effect of Rotation Speed

It is well accepted that the higher the rotation speed the better the diffusion rate of the oxygen. As such the effect of rotation speed of the two catalysts were studied both in alkaline and acid as shown in the figure below (Fig. 17)

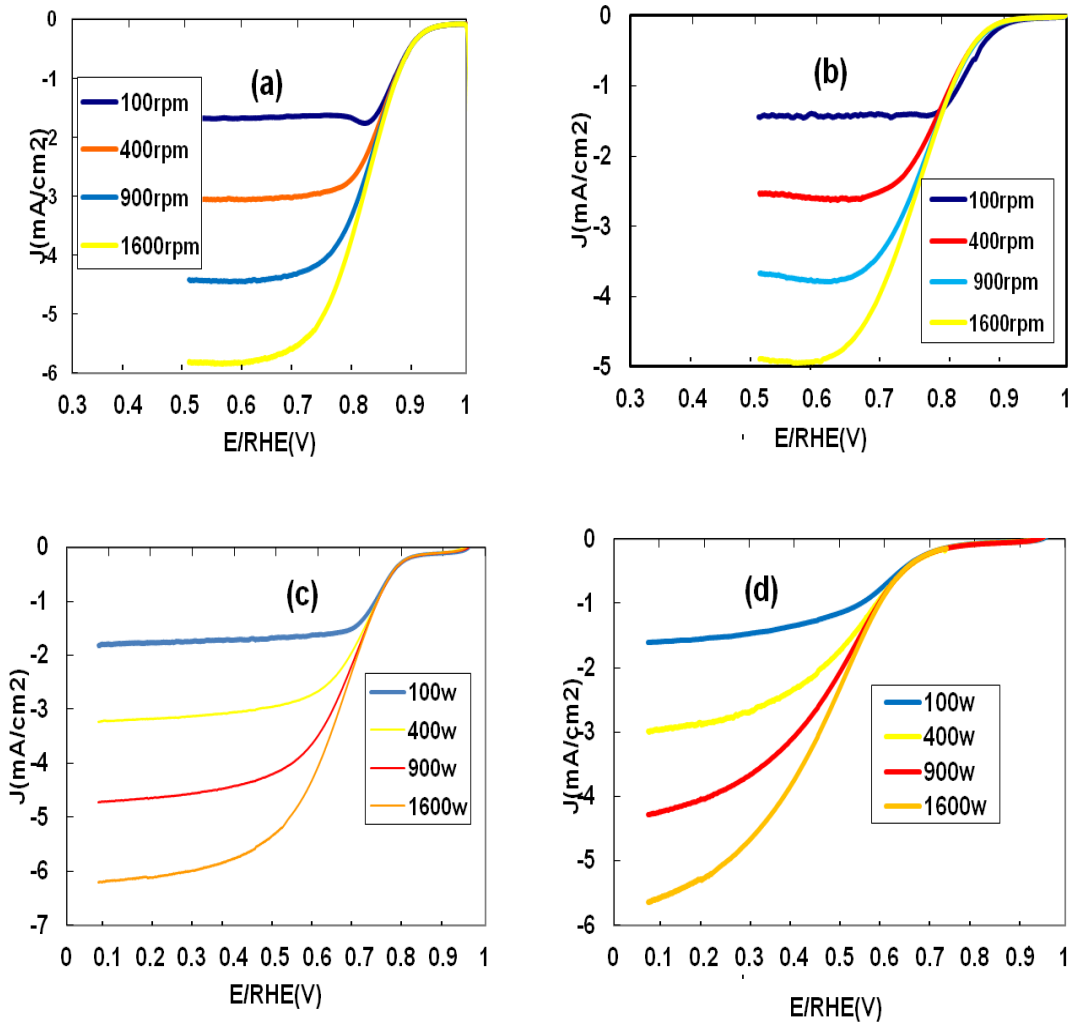

Figure 17: Rotation speed effect in: Alkaline (a) Fe-N-C/KB (b) Fe-N-C/Vul and Acid (c) Fe-N-C/KB (d) Fe-N-C/Vul

As can be observed from the figures above, Levich principle is well respected for the two catalysts in the two media

4.8.5 Comparison between the Catalysts and Platinum

The activities of the two catalysts were also compared to that of conventional Pt/C (26.5µg/Pt loading) in both alkaline and acidic media as shown in the figure below (Fig. 18). Figure 18a shows activity of Fe-N-C/KB in alkaline solution. The ORR characteristic of our Fe-N-C/KB catalyst is quite superior to that of Pt/C, especially in the kinetic region between 0.75 and 0.85V/RHE. Also, Fe-N-C/KB catalyst seems to outperform Pt/C in the diffusion regime. Such small difference in catalytic behavior could be interpreted as follows: (i) it is well known that hydrogen peroxide can be produced on Pt at voltage below 0.6V/RHE thereby decreasing the limiting current[30]; (ii) high loading of Fe-N-C catalyst can enhance activity due to the availability of more active sites for ORR. Consequently, the H_2O_2 thus produced is reduced to water on the catalyst surface.[31] However, Fe-N-C/KB in acidic medium shows an activity lower than

that of Pt/c by 90mV and 130mV at onset and half-wave potentials, respectively.

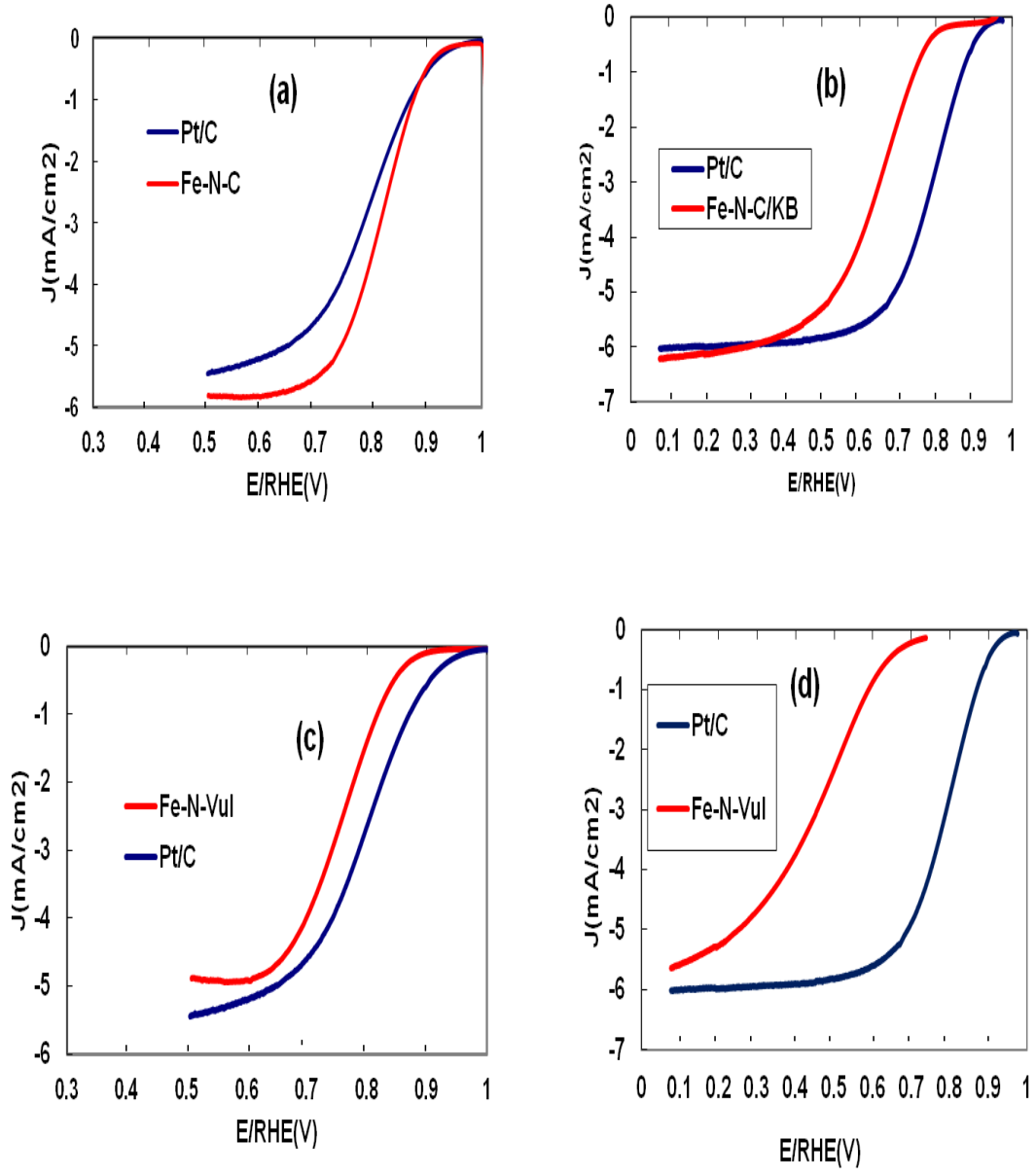

Figure 18: ORR curves in O_2 saturated of :Fe-N-C/KB (a) Alkaline (b) Acid and Fe-N-C/Vul (c) Alkaline (d) Acid

As for Fe-N-C/Vul, Pt/C outperforms, both in kinetic and diffusion region in the two media.

4.8.6 Catalyst durability

The two catalysts showed not only remarkable activity, but also good stability after subjecting it to prolonged potential cycling between 0.65 and 1.0 V/RHE using square-wave signal of 5s at each interval in accordance with the DOE protocol. ORR activity was evaluated in fresh oxygen saturated 0.1 M KOH solution after every 5000 cycles.

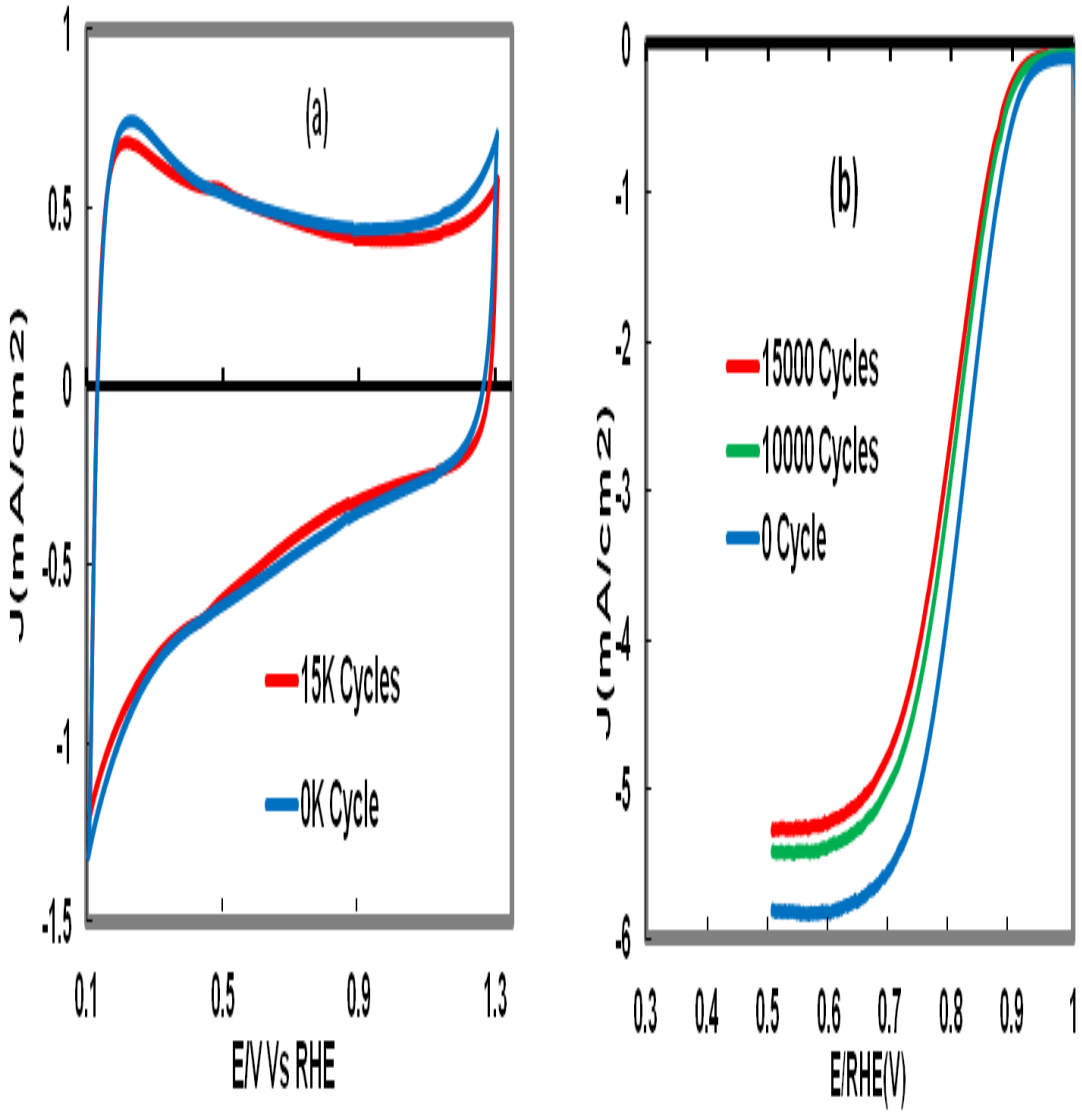

Figure 19: Stability Test for Fe-N-C/KB (a) Cyclic Voltammetry in N_2 saturated 0.1MKOH (b) Linear Voltammetry in O_2 saturated 0.1MKOH

At a constant current density of -3mA/cm^2 (approximately half-wave potential), the drop in voltage corresponding to 10,000 and 15,000 cycles was estimated to be 21 and 9mV respectively (Figure 19). This means that the degradation rate dropped from 2.1μV/cycle in the first 10,000 cycles to 1.8μV/cycle in the last 5,000 cycles. Such a trend in activity loss over cycling has also been seen with conventional Pt/C catalyst, where most of ORR overvoltage occurs in the first 5k-10k cycles, after which the activity stabilizes somewhat. For the Pt/C catalyst, activity degradation is largely due to the loss in surface area as a result of particle growth.[47] In the case of Fe-N-C, however, the activity loss could be ascribed to: (i) iron oxidation/dissolution. This has been confirmed by measuring the activity of the catalyst before and after acid treatment which indicates that iron leaching caused significant drop in the activity. (ii) Stability of nitrogen functionalities on carbon surface. It is generally accepted that a composite with high nitrogen content is capable of creating more active sites which gives rise to higher ORR activity.[48]

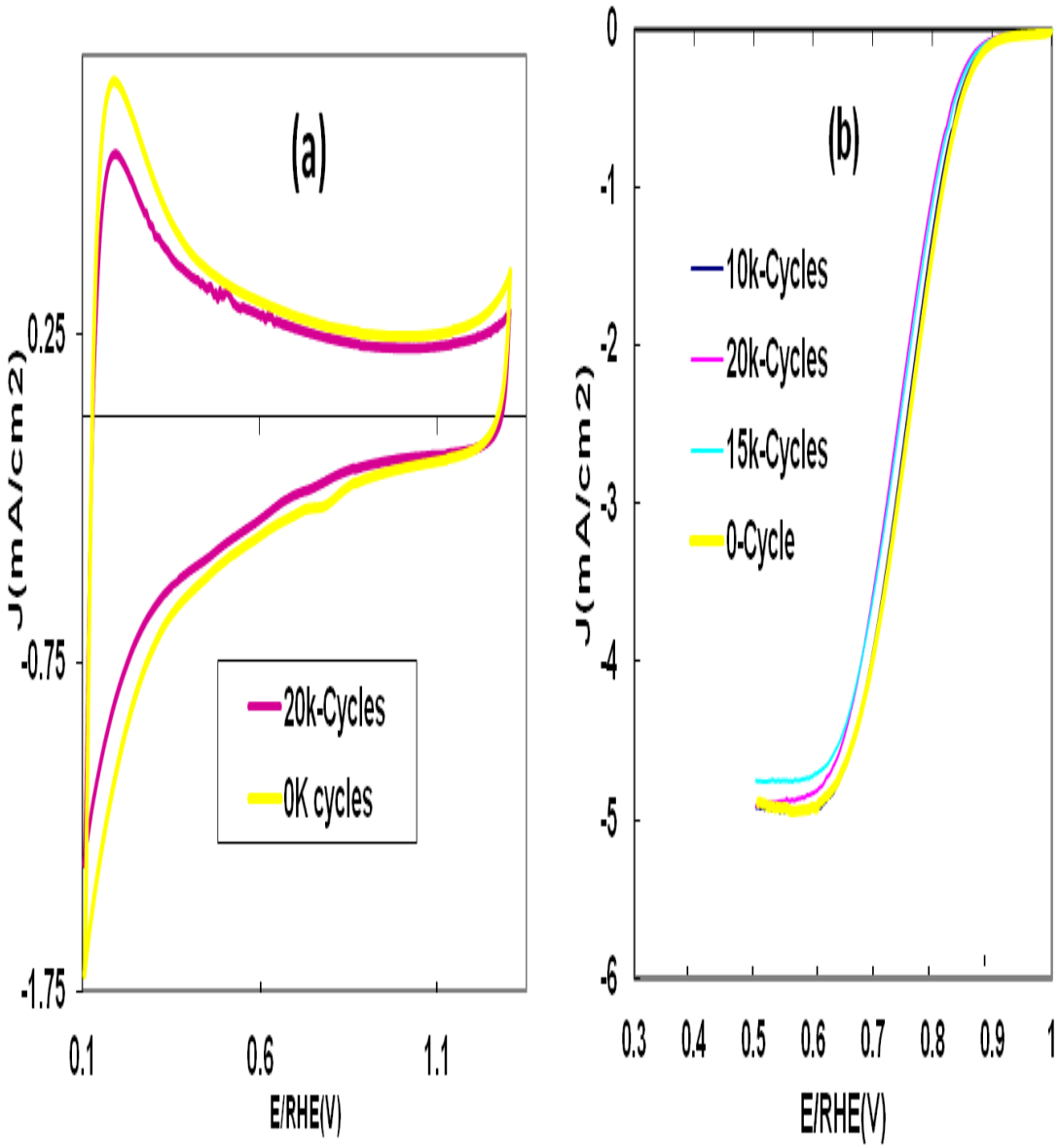

Figure 20: Stability Test for Fe-N-C/Vul (a) Cyclic Voltammetry in N_2 saturated 0.1MKOH (b) Linear Voltammetry in O_2 saturated 0.1MKOH

However, Fe-N-C/Vul does not really show any significant degradation even after prolonged cycling.

It is worth mentioning that up to now there is no clear evidence about the type of nitrogen that would make the catalyst more stable under potential cycling in a specific electrolyte. This is due to the difficulty in finding a suitable synthesis method that would lead to a specific type of nitrogen function. Any nitrogen precursor used for the synthesis of Pt-free catalysts, always resulted in catalyst with different nitrogen functionalities mentioned above. Therefore, we assume the remarkable stability of our catalysts, Fe-N-C/KB and Fe-N-C/Vul could be associated with high content of pyrrolic nitrogen which is not vulnarable to degradation in alkaline medium.

4.8.7 Methanol Tolerance

Furthermore, having a catalyst that is active toward ORR at the cathode but inert to methanol oxidation is of great relevance to direct methanol fuel cell (DMFC) applications, where it is crucial to keep cathode performance unchanged, particularly during the cross-over of methanol to cathode side. Therefore, measurements were carried out to demonstrate the inactivity of the synthesized Fe-N-C catalyst towards methanol oxidation.

As shown in Figure 21, the ORR activity of the catalysts remained unaffected even in the presence of 0.5M methanol, in good agreement with reported work in literature.[30]

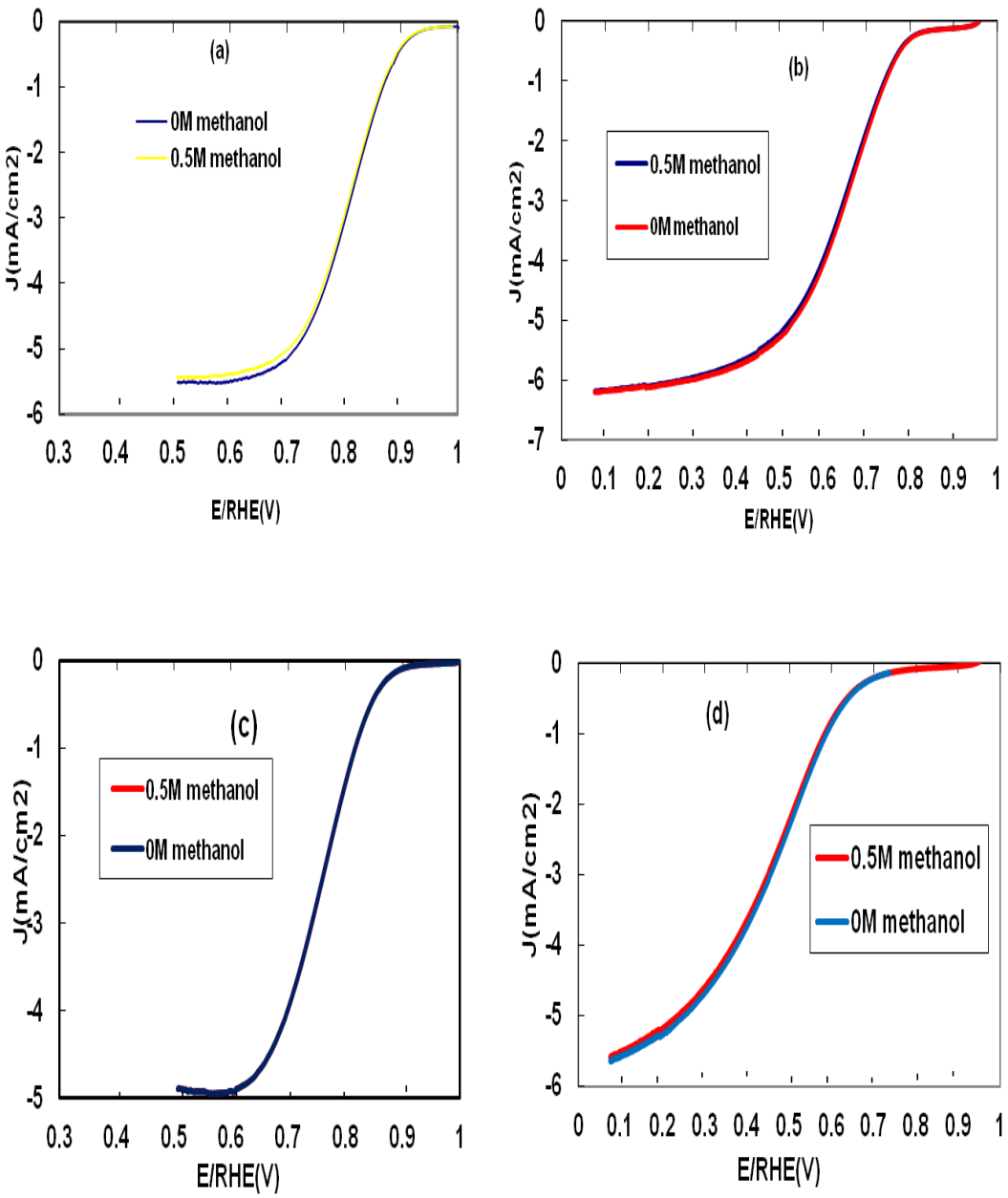

Figure 21: Methanol Tolerance curves in O_2 saturated for: Fe-N-C/KB in (a) Alkaline (b) Acid and Fe-N-C/Vul in (c) Alkaline (d) Acid

4.8.7 Effect of Metal

The catalytic activity of electrocatalysts compounds towards ORR strongly depends on the individual transition metal center and the macrocyclic ligand, as well as the size of the π electron system. In this regard, we evaluated the effect of two different metals namely cobalt and iron as shown in the figure below.

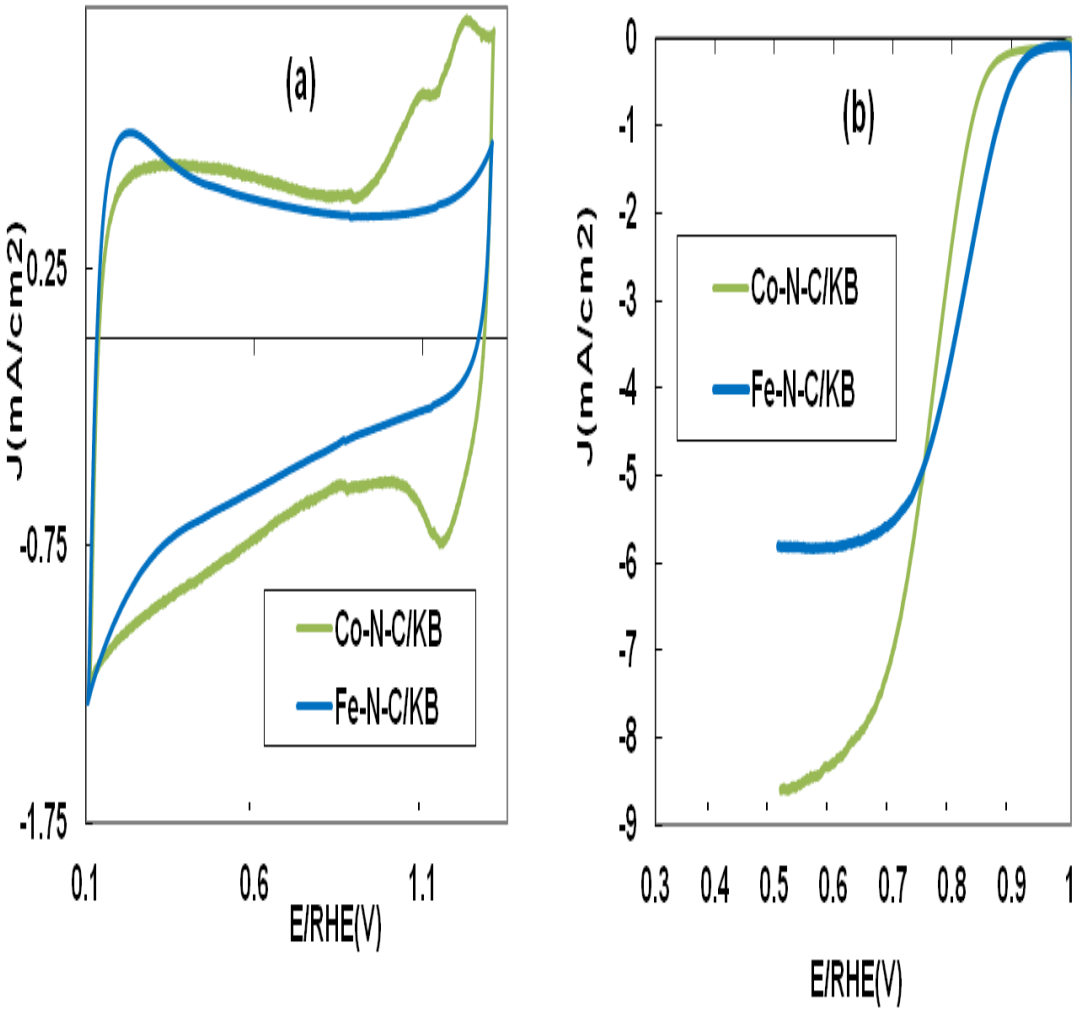

Figure 22: (a) Cyclic Voltammetry curve N_2 saturated 0.1KOH of Co-N-/KB and Fe-N-C/KB (a) ORR curve of O2 saturated 0.1KOH of Co-N-/KB and Fe-N-C/KB

Based on capacitive envelop (CV) as seen in the Figure 22a, Co-N-/KB has similar BET area with some redox system at 1.1V which can be attributed to the couple Co^{II}/Co^{III}. However, this catalyst does not perform as the one based on iron (Fig. 22b). Fe-N-C/KB has better intrinsic electrocatalytic properties than Co-N-/KB. This was displayed in Figure 22b where it has better activity in the kinetic region than Co-N-/KB. This trend actually corroborates what has been reported in the literature that the activity of electrocatalytic compounds changes with respect to the central metal ions in the following order: Fe> Co> Ni> Cu.[4] Surprisingly, in the limiting current region, Co-N-C/Kb shows a very high current density. This is unexpected behavior and needs more investigation to understand the mechanism.

Conclusion

The research was conducted successfully and the followings are its scientific outcomes :

1. A novel vinazene-based nitrogen precursor was used for the first time to synthesize a highly active Fe-N-C electrocatalysts for ORR by a simple and environmentally friendly approach.
2. Pyrolysis of vinazene-carbon composite led to a catalyst rich in pyrrolic nitrogen function and high ORR activity.
3. Systematic experiments have led us to demonstrate that it is not only the graphitic nitrogen that is responsible for high ORR activity, but also the *pyrrolic* nitrogen as confirmed by the activity of our catalyst, Fe-N-C/KB (rich in pyrrolic nitrogen).
4. One of the synthesized catalysts (Fe-N-C/KB) demonstrated a Pt-like behavior in alkaline medium.

5. Their excellent stability under prolonged cycling and tolerance towards methanol oxidation make them promising candidates for air electrode, in both fuel cells and batteries.

Recommendation

The followings are suggested for future work:

1. The use of vinazene with other nitrogen source as blend (such as polyaniline, melamine, phenanthroline, polypyrrole) could be a means of achieving high Fe/N doped carbon.
2. Real cell application testing of the synthesized catalysts
3. Variation of elemental ratio of the synthesized catalysts to establish optimum percentage for each element in the catalyst.
4. Effect of heat treatment temperature variation to establish optimum temperature for heat treatment.
5. Incorporation of metal oxide (e.g WOx, MnOx) into the catalysts to act as peroxide scavenger.

References

(1) Zaidi, S. J.; Rauf, M. A. *Fuel cell fundamentals*; Springer, 2009.
(2) Yan, Q.; Toghiani, H.; Causey, H. *Journal of Power Sources* **2006**, *161*, 492.
(3) Iojoiu, C.; Chabert, F.; Maréchal, M.; Kissi, N. E.; Guindet, J.; Sanchez, J.-Y. *Journal of Power Sources* **2006**, *153*, 198.
(4) Song, C.; Zhang, J. In *PEM fuel cell electrocatalysts and catalyst layers*; Springer, 2008.
(5) Sasaki, K.; Naohara, H.; Choi, Y.; Cai, Y.; Chen, W.-F.; Liu, P.; Adzic, R. R. *Nat Commun* **2012**, *3*, 1115.
(6) Stamenkovic, V. R.; Fowler, B.; Mun, B. S.; Wang, G.; Ross, P. N.; Lucas, C. A.; Marković, N. M. *Science* **2007**, *315*, 493.
(7) Chen, R.; Li, H.; Chu, D.; Wang, G. *The Journal of Physical Chemistry C* **2009**, *113*, 20689.
(8) Jasinski, R. **1964**.
(9) Yeager, E. *Journal of Molecular Catalysis* **1986**, *38*, 5.
(10) Taylor, R. J.; Humffray, A. A. *Journal of Electroanalytical Chemistry and Interfacial Electrochemistry* **1975**, *64*, 85.
(11) Appel, M.; Appleby, A. J. *Electrochimica Acta* **1978**, *23*, 1243.
(12) Morcos, I.; Yeager, E. *Electrochimica Acta* **1970**, *15*, 953.
(13) Paliteiro, C.; Hamnett, A.; Goodenough, J. B. *Journal of Electroanalytical Chemistry and Interfacial Electrochemistry* **1987**, *233*, 147.
(14) Jürmann, G.; Tammeveski, K. *Journal of Electroanalytical Chemistry* **2006**, *597*, 119.
(15) Jahnke, H.; Schonborn, M.; Zimmermann, G. *Top Curr Chem* **1976**, *61*, 133.
(16) Maldonado, S.; Stevenson, K. J. *J Phys Chem B* **2005**, *109*, 4707.
(17) Sidik, R. A.; Anderson, A. B.; Subramanian, N. P.; Kumaraguru, S. P.; Popov, B. N. *The Journal of Physical Chemistry B* **2006**, *110*, 1787.
(18) Gong, K.; Du, F.; Xia, Z.; Durstock, M.; Dai, L. *Science* **2009**, *323*, 760.
(19) Qu, L.; Liu, Y.; Baek, J.-B.; Dai, L. *ACS nano* **2010**, *4*, 1321.
(20) Yang, Z.; Yao, Z.; Li, G.; Fang, G.; Nie, H.; Liu, Z.; Zhou, X.; Chen, X. a.; Huang, S. *ACS nano* **2011**, *6*, 205.
(21) Morozan, A.; Jégou, P.; Campidelli, S.; Palacin, S.; Jousselme, B. *Chemical Communications* **2012**, *48*, 4627.
(22) Unni, S. M.; Devulapally, S.; Karjule, N.; Kurungot, S. *Journal of Materials Chemistry* **2012**, *22*, 23506.
(23) Shin, D.; Jeong, B.; Mun, B. S.; Jeon, H.; Shin, H.-J.; Baik, J.; Lee, J. *The Journal of Physical Chemistry C* **2013**, *117*, 11619.
(24) Jeon, I.-Y.; Choi, H.-J.; Choi, M.; Seo, J.-M.; Jung, S.-M.; Kim, M.-J.; Zhang, S.; Zhang, L.; Xia, Z.; Dai, L. *Scientific Reports* **2013**, *3*.
(25) Zagal, J.; Sen, R. K.; Yeager, E. *Journal of Electroanalytical Chemistry and Interfacial Electrochemistry* **1977**, *83*, 207.
(26) Shigehara, K.; Anson, F. C. *The Journal of Physical Chemistry* **1982**, *86*, 2776.
(27) Liu, H. Y.; Weaver, M. J.; Wang, C. B.; Chang, C. K. *Journal of Electroanalytical Chemistry and Interfacial Electrochemistry* **1983**, *145*, 439.
(28) Shi, C.; Anson, F. C. *Inorganic chemistry* **1990**, *29*, 4298.

(29) Zhang, L.; Zhang, J.; Wilkinson, D. P.; Wang, H. *Journal of Power Sources* **2006**, *156*, 171.
(30) Li, Y.; Zhou, W.; Wang, H.; Xie, L.; Liang, Y.; Wei, F.; Idrobo, J.-C.; Pennycook, S. J.; Dai, H. *Nature nanotechnology* **2012**, *7*, 394.
(31) Merzougui, B.; Hachimi, A.; Akinpelu, A.; Bukola, S.; Shao, M. *Electrochimica Acta* **2013**, *107*, 126.
(32) (a) Liang, Y.; Li, Y.; Wang, H.; Zhou, J.; Wang, J.; Regier, T.; Dai, H. *Nat Mater* **2011**, *10*, 780(b) Wu, G.; More, K. L.; Johnston, C. M.; Zelenay, P. *Science* **2011**, *332*, 443.
(33) (a) Chen, Z.; Higgins, D.; Yu, A.; Zhang, L.; Zhang, J. *Energy & Environmental Science* **2011**, *4*, 3167(b) Jaouen, F.; Proietti, E.; Lefèvre, M.; Chenitz, R.; Dodelet, J.-P.; Wu, G.; Chung, H. T.; Johnston, C. M.; Zelenay, P. *Energy & Environmental Science* **2011**, *4*, 114.
(34) Li, W.; Yu, A.; Higgins, D. C.; Llanos, B. G.; Chen, Z. *Journal of the American Chemical Society* **2010**, *132*, 17056.
(35) Bezerra, C. W.; Zhang, L.; Lee, K.; Liu, H.; Marques, A. L.; Marques, E. P.; Wang, H.; Zhang, J. *Electrochimica Acta* **2008**, *53*, 4937.
(36) Gewirth, A. A.; Thorum, M. S. *Inorganic chemistry* **2010**, *49*, 3557.
(37) (a) Meier, H.; Tschirwitz, U.; Zimmerhackl, E.; Albrecht, W.; Zeitler, G. *The Journal of Physical Chemistry* **1977**, *81*, 712(b) Tanaka, A.; Fierro, C.; Scherson, D.; Yaeger, E. *Journal of Physical Chemistry* **1987**, *91*, 3799.
(38) Proietti, E.; Jaouen, F.; Lefèvre, M.; Larouche, N.; Tian, J.; Herranz, J.; Dodelet, J.-P. *Nat Commun* **2011**, *2*, 416.
(39) Hosogai, T. Chem. Abstr, 1975; p 170924g.
(40) Rasmussen, P. G.; Reybuck, S. E.; Johnson, D. M.; Lawton, R. G.; Google Patents, 2000.
(41) (a) Beaujuge, P. M.; Fréchet, J. M. *Journal of the American Chemical Society* **2011**, *133*, 20009(b) Walker, B.; Han, X.; Kim, C.; Sellinger, A.; Nguyen, T.-Q. *ACS Applied Materials & Interfaces* **2012**, *4*, 244.
(42) Johnson, D. M.; Rasmussen, P. G. *Macromolecules* **2000**, *33*, 8597.
(43) Fu, L.; You, S.-J.; Zhang, G.-Q.; Yang, F.-L.; Fang, X.-H.; Gong, Z. *Biosensors and Bioelectronics* **2011**, *26*, 1975.
(44) Yasuda, S.; Yu, L.; Kim, J.; Murakoshi, K. *Chemical Communications* **2013**, *49*, 9627.
(45) (a) Cheon, J. Y.; Kim, T.; Choi, Y.; Jeong, H. Y.; Kim, M. G.; Sa, Y. J.; Kim, J.; Lee, Z.; Yang, T.-H.; Kwon, K.; Terasaki, O.; Park, G.-G.; Adzic, R. R.; Joo, S. H. *Sci. Rep.* **2013**, *3*(b) Subramanian, N. P.; Kumaraguru, S. P.; Colon-Mercado, H.; Kim, H.; Popov, B. N.; Black, T.; Chen, D. A. *Journal of Power Sources* **2006**, *157*, 56.
(46) (a) Zhang, J.; He, D.; Su, H.; Chen, X.; Pan, M.; Mu, S. *Journal of Materials Chemistry A* **2014**, *2*, 1242(b) Parvez, K.; Yang, S.; Hernandez, Y.; Winter, A.; Turchanin, A.; Feng, X.; Müllen, K. *ACS nano* **2012**, *6*, 9541(c) Yang, S.; Feng, X.; Wang, X.; Müllen, K. *Angewandte Chemie International Edition* **2011**, *50*, 5339.
(47) Ma, X.; Meng, H.; Cai, M.; Shen, P. K. *Journal of the American Chemical Society* **2012**, *134*, 1954.

(48) Zhang, Y.; Ge, J.; Wang, L.; Wang, D.; Ding, F.; Tao, X.; Chen, W. *Sci. Rep.* **2013**, *3*.

Vitae

Name	:Adeola Akeem Akinpelu
Nationality	:Nigeria
Date of Birth	:5/12/1982
Email	:oyonile@yahoo.com
Address	:O.T.M Mosque Boluwaji Ibadan Nigeria
Academic Background	:Usman Danfodio University Sokoto, Nigeria (B.sc Chemistry 2007)